The Liverwort, Marchantia, Drives Alternative Electron Flow Using a Flavodiiron Protein to Protect PSI

Shimakawa, Ginga ; Ishizaki, Kimitsune ; Tsukamoto, Shigeyuki ; Tanaka, Moeko ; Sejima, Takehiro ; Miyake, Chikahiro

(Citation)
Plant Physiology,173(3):1636-1647

(Issue Date)
2017-03

(Resource Type)
journal article

(Version)
Version of Record

The Liverwort, *Marchantia*, Drives Alternative Electron Flow Using a Flavodiiron Protein to Protect PSI[1][OPEN]

Ginga Shimakawa[2], Kimitsune Ishizaki[2], Shigeyuki Tsukamoto, Moeko Tanaka, Takehiro Sejima, and Chikahiro Miyake*

Graduate School of Agricultural Science (G.S., M.T., T.S., C.M.) and Graduate School of Science (K.I., S.T.), Kobe University, Nada, Kobe 657-8501, Japan; and Core Research for Environmental Science and Technology, Japan Science and Technology Agency, Chiyoda-ku, Tokyo 102-0076, Japan (C.M.)

ORCID IDs: 0000-0002-8557-2096 (G.S.); 0000-0003-0504-8196 (K.I.); 0000-0002-5318-3707 (M.T.); 0000-0002-2426-2377 (C.M.).

The diffusion efficiency of oxygen in the atmosphere, like that of CO_2, is approximately 10^4 times greater than that in aqueous environments. Consequently, terrestrial photosynthetic organisms need mechanisms to protect against potential oxidative damage. The liverwort *Marchantia polymorpha*, a basal land plant, has habitats where it is exposed to both water and the atmosphere. Furthermore, like cyanobacteria, *M. polymorpha* has genes encoding flavodiiron proteins (FLV). In cyanobacteria, FLVs mediate oxygen-dependent alternative electron flow (AEF) to suppress the production of reactive oxygen species. Here, we investigated whether FLVs are required for the protection of photosynthesis in *M. polymorpha*. A mutant deficient in the FLV1 isozyme (Δ*MpFlv1*) sustained photooxidative damage to photosystem I (PSI) following repetitive short-saturation pulses of light. Compared with the wild type (Takaragaike-1), Δ*MpFlv1* showed the same photosynthetic oxygen evolution rate but a lower electron transport rate during the induction phase of photosynthesis. Additionally, the reaction center chlorophyll in PSI, P700, was highly reduced in Δ*MpFlv1* but not in Takaragaike-1. These results indicate that the gene product of *MpFlv1* drives AEF to oxidize PSI, as in cyanobacteria. Furthermore, FLV-mediated AEF supports the production of a proton motive force to possibly induce the nonphotochemical quenching of chlorophyll fluorescence and suppress electron transport in the cytochrome b_6/f complex. After submerging the thalli, a decrease in photosystem II operating efficiency was observed, particularly in Δ*MpFlv1*, which implies that species living in these sorts of habitats require FLV-mediated AEF.

A decrease in the efficiency of light usage for photosynthetic CO_2 fixation in the Calvin-Benson cycle enhances the likelihood that oxygenic phototrophs will suffer from photooxidative damage caused by reactive oxygen species (ROS; Miyake, 2010). For example, under conditions of high light, low CO_2, and/or low temperature, the light energy absorbed by PSI and PSII in thylakoid membranes exceeds requirements, because turnover of the Calvin-Benson cycle limits the regeneration of $NADP^+$. Consequently, electrons accumulate in the photosynthetic electron transport (PET) system. The accumulated electrons start to flow to oxygen, producing ROS, including superoxide anion radicals and hydrogen peroxide, in PSI (Krieger-Liszkay, 2005; Sejima et al., 2014; Zivcak et al., 2015a, 2015b; Takagi et al., 2016). Furthermore, the accumulation of electrons in the PET system suppresses the charge separation of the reaction center chlorophylls (Chls), P680 in PSII and P700 in PSI, which stimulates the production of another ROS, singlet oxygen (Cazzaniga et al., 2012; Fischer et al., 2013). It is proposed that the reduced state of P700 in PSI under illuminated conditions stimulates the production of singlet oxygen and superoxide anion radicals to inactivate PSI, resulting in a decline in photosynthetic CO_2 fixation (Cazzaniga et al., 2012; Rutherford et al., 2012; Sejima et al., 2014; Zivcak et al., 2015a, 2015b; Takagi et al., 2016).

Oxygenic phototrophs have various systems that can be used to suppress electron accumulation in the PET system; they are broadly divided into two groups. The first group uses regulation of the absorption efficiency of photon energy into the PET system, which includes nonphotochemical quenching (NPQ) of Chl fluorescence and state transition (Derks et al., 2015). In the second group, electron sinks consume excess photon energy as futile electron pathways with heat dissipation. These

[1] This work was supported by the Japan Society for the Promotion of Science (grant no. 26450079 to C.M. and grant no. 16J03443 to G.S.) and by the Core Research for Evolutional Science and Technology division of the Japan Science and Technology Agency (grant no. AL65D21010 to C.M.).

[2] These authors contributed equally to the article.

* Address correspondence to cmiyake@hawk.kobe-u.ac.jp.

The author responsible for distribution of materials integral to the findings presented in this article in accordance with the policy described in the Instructions for Authors (www.plantphysiol.org) is: Chikahiro Miyake (cmiyake@hawk.kobe-u.ac.jp).

C.M. conceived the original screening and research plans; C.M. and K.I. supervised the experiments; G.S. performed most of the experiments; K.I., S.T., M.T., and T.S. provided technical assistance to G.S.; C.M. and G.S. designed the experiments and analyzed the data; C.M. and G.S. conceived the project and wrote the article with contributions from all the authors; C.M. supervised and complemented the writing.

[OPEN] Articles can be viewed without a subscription.

www.plantphysiol.org/cgi/doi/10.1104/pp.16.01038

electron sinks constitute alternative electron flow (AEF), and the representatives are observed as photorespiration and Mehler-like reactions (Kozaki and Takeba, 1996; Asada, 1999; Helman et al., 2003; Takahashi et al., 2007; Hayashi et al., 2014; Shimakawa et al., 2015; Sejima et al., 2016).

With regard to the protection of PSI against photooxidative damage, there is a further strategy in addition to NPQ and AEF that suppresses photosynthetic electron transport in the cytochrome b_6/f complex in the center of the PET system. This suppression is triggered by the integration of a proton gradient across thylakoid membranes (ΔpH; Kramer et al., 1999) or the reduction of the plastoquinone (PQ) pool (Shaku et al., 2016), which contributes to the oxidation of PSI. Furthermore, ΔpH also is involved in the induction of the molecular mechanisms of some NPQ (Derks et al., 2015). Collectively, oxygenic phototrophs harbor many systems for the alleviation of photooxidative damage that are rich in diversity and have been acquired or lost by species over their evolutionary history.

One of the most enduring mysteries is whether a molecular mechanism of AEF has been lost over the long history of evolutionary processes in oxygenic phototrophs. In the progenitor cyanobacteria, Helman et al. (2003) found a large AEF to oxygen, which is not photorespiration, and showed that the AEF is driven by FLAVODIIRON PROTEIN1 (FLV1) and FLV3. Some cyanobacteria have four isozymes of FLV (FLV1−FLV4), whereas others have just two: FLV1 and FLV3. FLV1/3 and FLV2/4 function as heterodimers (Zhang et al., 2012; Allahverdiyeva et al., 2013). In *Synechocystis* sp. PCC 6803 (S. 6803), both FLV1/3 and FLV2/4 mediate oxygen-dependent AEF as well as oxidize the PET system under CO_2-saturated and CO_2-limited conditions, respectively (Helman et al., 2003; Hayashi et al., 2014; Shimakawa et al., 2015). An S. 6803 mutant deficient in FLV1/3 was shown to sustain oxidative damage under fluctuating light (Allahverdiyeva et al., 2013), and another mutant deficient in FLV2/4 also suffered under low-CO_2 conditions (Zhang et al., 2012). These data indicate that FLV is essential for the alleviation of photooxidative damage in cyanobacteria. Surprisingly, during the course of evolution, the isozymes of FLV have been lost in seed plants at the gene level (Yamamoto et al., 2016). On the basis of accumulated genomic information, FLV1/3 isozymes are found to be broadly conserved in the photosynthetic green plant lineage, including cyanobacteria, green algae, bryophytes, pteridophytes, and pinophytes; there is more sequence variation between basal land plants and cyanobacteria than there is among cyanobacteria (Yamamoto et al., 2016). This suggests that, at some point in the course of evolution, oxygenic phototrophs no longer had a need for FLV. However, the physiological functions of FLV in phototrophs other than cyanobacteria have yet to be elucidated.

The liverwort *Marchantia polymorpha* is positioned between algae and plants in the photosynthetic green plant lineage (Bowman et al., 2007) and has two genes encoding isozymes of FLV1/3 (*MpFlv1* [*Mapoly0005s0210*] and *MpFLV3* [*Mapoly0103s0039*]). Additionally, one of the habitats of *M. polymorpha* is the marginal area between aquatic and land environments; thus, this plant sometimes experiences both submergence and drought stress. Submergence limits the diffusion of gases. The diffusion coefficient of CO_2 in water is approximately 10^{-4} times lower than that in the atmosphere, which depresses photosynthetic CO_2 fixation (Raven et al., 1985; Badger and Spalding, 2000). Furthermore, another habitat of the liverwort is the forest floor, where photon energy from the sun is provided as fluctuating light termed sunfleck (Boardman, 1977). These habitat situations suggest that *M. polymorpha* would require sufficient AEF activity to escape from oxidative damage through the dissipation of excess photon energy.

In this study, we sought to clarify the physiological functions of FLV in *M. polymorpha* by comparing the wild type (Takaragaike-1 [Tak-1]) and a mutant deficient in *MpFlv1* (Δ*MpFlv1*). We found that the activity of AEF was mediated by FLV, which supports the formation of ΔpH that contributes to the protection of PSI against photooxidative damage under the fluctuating light conditions in which *M. polymorpha* grows.

RESULTS AND DISCUSSION

Effects of FLV on Photooxidative Damage to PSI in *M. polymorpha*

We constructed the mutant Δ*MpFlv1* through targeted disruption of the gene *MpFlv1* (Supplemental Fig. S1). We found that the maximum quantum efficiency of PSII photochemistry (F_v/F_m) in Δ*MpFlv1* was not different from that of the wild-type Tak-1 or of the complement mutant to Δ*MpFlv1* (c*MpFlv1*; Table I). Additionally, total amounts of Chl *a* and *b* were almost the same among these plants (Table I). Furthermore, the total nitrogen content of Δ*MpFlv1* also was at the same level as those in Tak-1 and c*MpFlv1* (Table I). These data indicate that the deletion of *MpFlv1* has little effect on the growth of *M. polymorpha* under the growth conditions used in this study.

To investigate the physiological functions of FLV in the protection of PSI and PSII in *M. polymorpha*, we illuminated the thalli of Tak-1, Δ*MpFlv1*, and c*MpFlv1* with short-saturation pulses. Repetitive short-saturation pulse (rSP) illumination saturates the PET system with electrons to selectively inactivate PSI, with oxygen required in C_3 plant leaves (Sejima et al., 2014; Zivcak et al., 2015a, 2015b). In sunflower (*Helianthus annuus*) leaves, total oxidizable P700 (P_m) decreased to about 10% of the initial value through rSP treatment (300 ms, 20,000 μmol photons m^{-2} s^{-1}, every 10 s) for 4 h, whereas F_v/F_m decreased to about 80% (Sejima et al., 2014). Hence, rSP treatment is a useful method of inducing the photoinhibition of PSI in vivo and of investigating the robustness of PSI against photooxidative damage.

In Δ*MpFlv1*, rSP treatment (1 s, 3,000 μmol photons m^{-2} s^{-1}, every 10 s) significantly decreased both

Table I. *Characteristics of Tak-1, ΔMpFlv1, and cMpFlv1*

Data are shown as means ± SD of three independent measurements.

Plant	F_v/F_m	Total Chl	Chl *a*/Chl *b*	Total Nitrogen
		$g\ m^{-2}$		$g\ m^{-2}$
Tak-1	0.811 ± 0.008	0.20 ± 0.03	2.97 ± 0.12	0.79 ± 0.12
Δ*MpFlv1*	0.804 ± 0.004	0.20 ± 0.01	3.08 ± 0.04	0.76 ± 0.06
c*MpFlv1*	0.803 ± 0.018	0.22 ± 0.04	3.03 ± 0.08	0.73 ± 0.11

P_m and F_v/F_m, as compared with its effect in Tak-1 (Fig. 1), which suggests that photoinhibition of PSI and PSII occurs during rSP treatment in Δ*MpFlv1*. Posttreatment P_m and F_v/F_m were measured after a 30-min incubation in the dark to relax the influence of NPQ, state transition, and chloroplast movements. Complementation of Δ*MpFlv1* with *MpFlv1* partially relieved the photoinhibition of both PSI and PSII (Fig. 1). In Δ*MpFlv1*, the degree of decrease in P_m was greater than that in F_v/F_m (Fig. 1), indicating that, in liverworts as in C_3 plants, rSP treatment leads to photooxidative damage mainly in PSI (Sejima et al., 2014; Zivcak et al., 2015a, 2015b). Compared with rSP treatment in air, the extent of PSI damage was smaller in Δ*MpFlv1* during treatment in the absence of oxygen (Fig. 1A), which suggests that the photoinhibition of PSI in Δ*MpFlv1* is caused by ROS. In contrast, the decrease in F_v/F_m during rSP treatment was accelerated in the absence of oxygen (Fig. 1B). In PSII, oxygen-insensitive photodamage might occur during rSP treatment (Krause et al., 1985).

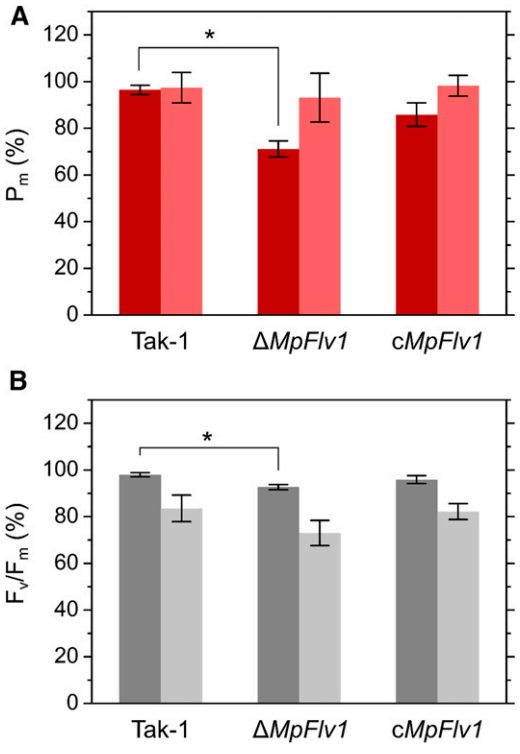

Figure 1. Effects of rSP treatment on P_m (A) and F_v/F_m (B) in Tak-1, Δ*MpFlv1*, and c*MpFlv1* in ambient air (dark-colored bars) and pure N_2 gas (light-colored bars). These values were obtained 30 min (in the dark) after 15-min treatments. For rSP treatments, rSPs (3,000 μmol photons $m^{-2}\ s^{-1}$, 1 s) were applied every 10 s in the dark. Data are represented as means ± SD of six independent measurements. Differences between Tak-1 and Δ*MpFlv1* were analyzed using Student's *t* test. Asterisks indicate statistically significant differences between Tak-1 and Δ*MpFlv1* at $P < 0.05$.

Effects of FLV on Photosynthesis in *M. polymorpha*

As shown in Figure 1A, FLV is required to protect PSI against photooxidative damage, which implies that the functions of FLV-mediated AEF in *M. polymorpha* are similar to those in cyanobacteria. To test this hypothesis, we simultaneously monitored oxygen exchange and the quantum yield of photochemical energy conversion in PSII (PSII operating efficiency), Y(II), in Tak-1, Δ*MpFlv1*, and c*MpFlv1* (Fig. 2). Before illumination with actinic light (AL), we determined dark respiration rates to be 1.5 ± 0.5, 1.7 ± 0.7, and 1.6 ± 0.5 μmol oxygen $m^{-2}\ s^{-1}$ in the thalli of Tak-1, Δ*MpFlv1*, and c*MpFlv1*, respectively ($n = 6$). Upon illumination of the thalli, gross photosynthetic oxygen evolution rates (net oxygen evolution rate + dark respiration rate) increased gradually during photosynthetic induction. Similar to Tak-1, Δ*MpFlv1* showed an induction of photosynthesis (Fig. 2A). Furthermore, c*MpFlv1* also showed the same rate of photosynthetic induction as Tak-1 and Δ*MpFlv1*. That is, the deficiency of *MpFlv1* did not affect photosynthesis. However, the behavior of Y(II) in these plants differed in the oxygen evolution rate during the induction of photosynthesis. In Tak-1, Y(II) started to increase before the increase in the oxygen evolution rate, just after the commencement of illumination (Fig. 2B). In contrast, in Δ*MpFlv1*, the increase in Y(II) was delayed and started to increase at 1 min after illumination was started. Y(II) in c*MpFlv1*, however, showed the same behavior as in Tak-1. These data indicate that, in *M. polymorpha*, the gene product of *MpFlv1* functions in AEF before the start of steady-state photosynthesis, which also is observed in the cyanobacterium S. 6803 (Supplemental Fig. S2). Both gross photosynthetic oxygen evolution rate and Y(II) in Δ*MpFlv1* reached the same values as those in Tak-1 and c*MpFlv1* at steady-state photosynthesis (Fig. 2). We evaluated the dependence of the gross photosynthetic oxygen evolution rate and Y(II) on photon flux density in Tak-1, Δ*MpFlv1*, and c*MpFlv1* (Supplemental Fig. S3). These data suggest that the effect of FLV on photosynthesis is smaller at steady state compared with the induction phase.

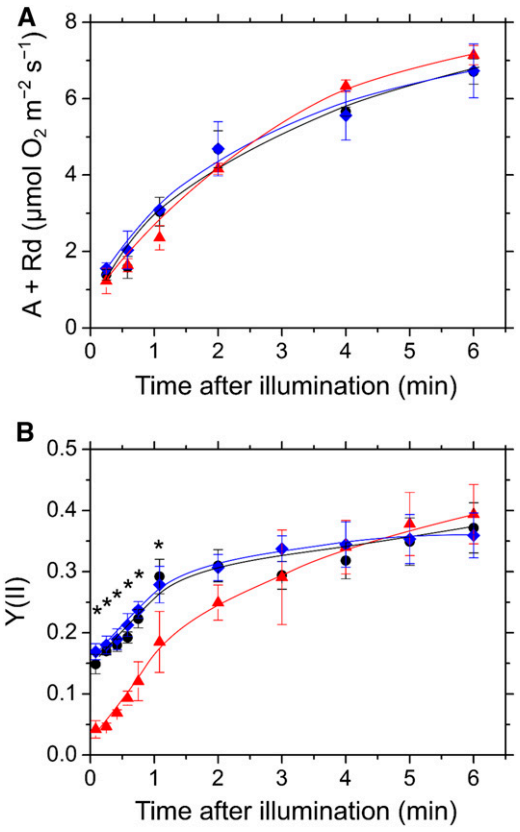

Figure 2. Time course of gross photosynthetic oxygen evolution rate (A; A) and Y(II) (B) in the induction phase of photosynthesis in Tak-1 (black circles), Δ*MpFlv1* (red triangles), and c*MpFlv1* (blue diamonds). Rd, Dark respiration rate. CO_2-saturated conditions were generated by adding 1 M $NaHCO_3$ to the felt mat in the reaction chamber. AL (200 μmol photons m^{-2} s^{-1}) was turned on at the zero time point. Data are represented as means ± SD of three independent measurements. Differences in Y(II) between Tak-1 and Δ*MpFlv1* were analyzed using Student's *t* test. Asterisks indicate statistically significant differences between Tak-1 and Δ*MpFlv1* at $P < 0.05$.

Effects of FLV on Photosynthetic Parameters in PSII and PSI in *M. polymorpha*

In *M. polymorpha*, the gene product of *MpFlv1* mediates AEF (Fig. 2), and its absence accelerates photooxidative damage to PSI (Fig. 1A). In plant leaves and cyanobacterial cells, photoinhibition of PSI is alleviated by the oxidation of P700, owing to a decrease in the amount of photooxidizable P700 (Sejima et al., 2014; Shimakawa et al., 2016b). These data indicate that FLV-mediated AEF contributes to the oxidation of P700 in *M. polymorpha*. To clarify the effects of FLV on the PET system in *M. polymorpha*, we investigated photosynthetic parameters in PSII and PSI in Tak-1, Δ*MpFlv1*, and c*MpFlv1* in the response to illumination with AL.

First, we examined the photosynthetic parameters in PSII using Chl fluorescence measurement. In both Tak-1 and c*MpFlv1*, Y(II) was higher than that in Δ*MpFlv1* during the induction phase of photosynthesis (Fig. 3A). Thereafter, the Y(II) in Δ*MpFlv1* became more similar to those in Tak-1 and c*MpFlv1* with photosynthesis induction (Fig. 3A). Additionally, compared with Δ*MpFlv1*, the observed NPQ also was higher in Tak-1 and c*MpFlv1* in response to illumination with AL (Fig. 3B). Furthermore, the coefficient of photochemical quenching of Chl fluorescence (qP) was higher in Tak-1 and c*MpFlv1* than in Δ*MpFlv1* (Fig. 3C). The light-response curves of Y(II), NPQ, and qP during steady-state photosynthesis also are shown (Fig. 4, A–C). Similar to Y(II), NPQ and qP had almost the same values at steady-state photosynthesis in these three plants, with the exception of illumination with high light leading to lower Y(II), NPQ, and qP in Δ*MpFlv1* than in Tak-1 and c*MpFlv1* (Fig. 4, A–C). Some of the discrepancy between Y(II) values depicted in Figure 4A and Supplemental Figure S3B might be due to differences in the equipment used to measure Chl fluorescence. Thus, we can draw the following tentative conclusions from the foregoing results. FLV drives photosynthetic linear electron flow as AEF, which would induce ΔpH to trigger NPQ (Derks et al., 2015). Both the stimulated electron sink and the enhanced NPQ caused by FLV-mediated AEF contribute to oxidation of the PET system, as demonstrated by the increase in qP (Figs. 3C and 4C; Miyake, 2008).

Next, we investigated the effects of FLV on the photosynthetic parameters in PSI, evaluated by examining changes in the absorbance of P700 (Klughammer and Schreiber, 1994; Schreiber and Klughammer, 2008). Similar to Y(II), we found higher quantum yields of PSI, Y(I), in Tak-1 and c*MpFlv1* than in Δ*MpFlv1* (Fig. 3D). We note that we cannot exclude the possibility that the deletion of FLV affects the distribution of PSII and PSI. Additionally, we measured the redox state of P700 in the induction phase of photosynthesis. Both Tak-1 and c*MpFlv1* showed larger donor-side limitation of PSI, Y(ND), than Δ*MpFlv1* (Fig. 3E), indicating that FLV-mediated AEF causes the Y(ND). In contrast, the acceptor-side limitations of PSI, Y(NA), were lower in Tak-1 and c*MpFlv1* than in Δ*MpFlv1* (Fig. 3F). That is, deletion of *MpFlv1* changed the limiting step from the donor side to the acceptor side of PSI. Thus, FLV contributes to the oxidation of P700 in the induction phase of photosynthesis in *M. polymorpha*, which might be responsible for the protection of PSI against photoinhibition (Fig. 1A). In c*MpFlv1*, lower Y(ND) and higher Y(NA) than those in Tak-1 were observed just after starting illumination (Fig. 3, E and F). The reason for this difference is unclear, but the recombinant gene product of *MpFlv1* in c*MpFlv1* might not function as well as the gene product expressed in Tak-1. The amount of the recombinant protein present in c*MpFlv1* also should be considered. The photosynthetic parameters, including Y(I), Y(ND), and Y(NA), in Δ*MpFlv1* changed in a time-dependent manner to reach almost the same values as those in Tak-1 and c*MpFlv1* at steady-state photosynthesis (Fig. 3, D–F). The light-response curves of Y(I), Y(ND), and Y(NA) during steady-state photosynthesis suggest that the contribution of FLV-mediated AEF to regulating the

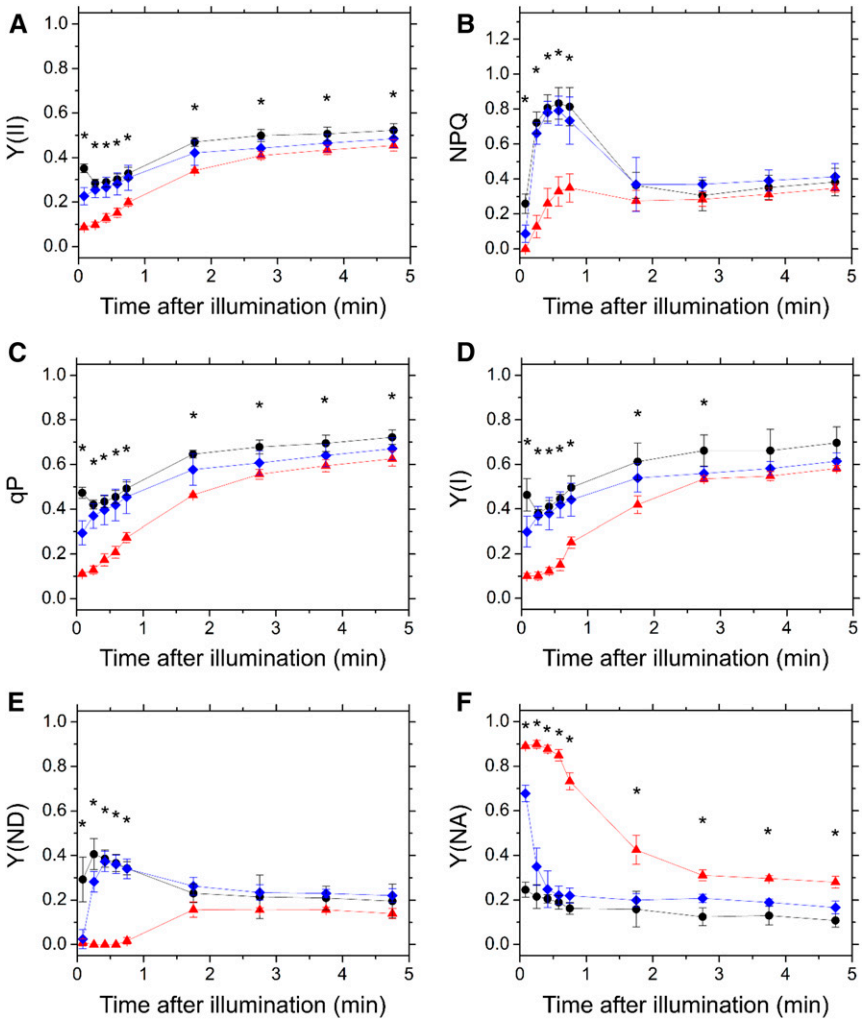

Figure 3. Time course of Y(II) (A), NPQ (B), qP (C), Y(I) (D), Y(ND) (E), and Y(NA) (F) in the induction phase of photosynthesis in Tak-1 (black circles), Δ*MpFlv1* (red triangles), and c*MpFlv1* (blue diamonds). AL (195 μmol photons m^{-2} s^{-1}) was turned on at the zero time point. Measurements were taken in ambient air. Data are represented as means ± SD of three independent measurements. Differences between Tak-1 and Δ*MpFlv1* were analyzed using Student's *t* test. Asterisks indicate statistically significant differences between Tak-1 and Δ*MpFlv1* at $P < 0.05$.

redox state of PSI is smaller at steady-state photosynthesis, compared with the induction phase, although significant differences were found between Tak-1 and Δ*MpFlv1* under high light (Fig. 4, D–F).

Furthermore, we measured photosynthetic parameters in PSII and PSI under a fluctuating light condition in Tak-1, Δ*MpFlv1*, and c*MpFlv1*. The thalli of these plants were illuminated with AL (200 μmol photons m^{-2} s^{-1}) to reach steady-state photosynthesis, and then we increased the photon flux density of AL by approximately 4-fold (840 μmol photons m^{-2} s^{-1}). During the transition from moderate to high light, Chl fluorescence and P700 absorbance were monitored simultaneously.

Both Y(II) and qP decreased in response to the transition to high light in all strains, with the largest decrease being observed in Δ*MpFlv1* (Fig. 5, A and C). Thereafter, lowered Y(II) and qP in Δ*MpFlv1* increased gradually to reach constant values approximately 4 min after the change in photon flux density, although both Y(II) and qP were initially maintained at constant levels in Tak-1 and c*MpFlv1* after the transition (Fig. 5, A and C). Additionally, the induction of NPQ by illumination with high light was retarded significantly in Δ*MpFlv1* compared with its induction in the other strains (Fig. 5B). The behaviors of these photosynthetic parameters in PSII were consistent with those in photosynthesis induction (Fig. 3, A–C).

In the case of PSI, the decrease in Y(I) during the transition from moderate to high light was largest in Δ*MpFlv1* (Fig. 5D), similar to the responses of Y(II) and qP (Fig. 5, A and C). In both Tak-1 and c*MpFlv1*, Y(ND) rose rapidly in response to high light and then decreased gradually to a constant level (Fig. 5E). However, Δ*MpFlv1* showed a slower induction of Y(ND) than was observed in Tak-1 and c*MpFlv1* (Fig. 5E). In contrast, a rapid increase in Y(NA) was observed in Δ*MpFlv1* during the transition to high light, whereas in Tak-1 and c*MpFlv1*, Y(NA) was not affected by the change in photon flux density (Fig. 5F). These data suggest that FLV-mediated AEF is required to maintain P700 in an oxidized state under fluctuating light in *M. polymorpha*, which is similar to observations of the cyanobacterium S. 6803 (Allahverdiyeva et al., 2013; Shimakawa et al., 2016b).

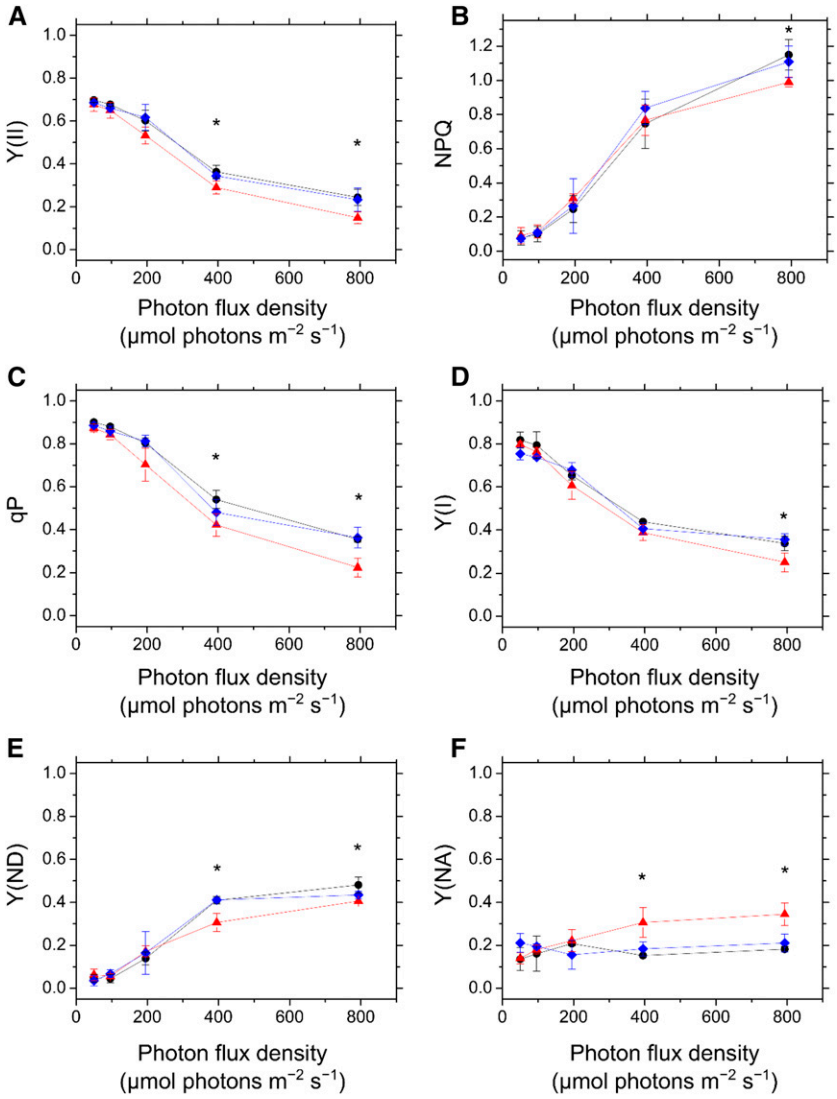

Figure 4. Dependence of Y(II) (A), NPQ (B), qP (C), Y(I) (D), Y(ND) (E), and Y(NA) (F) on photon flux density at steady-state photosynthesis in Tak-1 (black circles), Δ*MpFlv1* (red triangles), and c*MpFlv1* (blue diamonds). Measurements were taken in ambient air. Data are represented as means ± SD of three independent measurements. Differences between Tak-1 and Δ*MpFlv1* were analyzed using Student's *t* test. Asterisks indicate statistically significant differences between Tak-1 and Δ*MpFlv1* at $P < 0.05$.

Effects of FLV on Thylakoid Membrane Potential in *M. polymorpha*

To clarify the relationship between the FLV-mediated AEF and P700 oxidation, we evaluated the effects of FLV on thylakoid membrane potential in *M. polymorpha* by analyzing electrochromic shift (ECS, or P515, because the absorption measurements are made at 515 nm) signals (Klughammer et al., 2013) in the response to high light in Tak-1, Δ*MpFlv1*, and c*MpFlv1*. The ECS signal is considered an intrinsic optical voltmeter that responds rapidly to changes in the electrical potential across the thylakoid membrane (Witt, 1979) and can be utilized in a noninvasive spectroscopic measurement (Baker et al., 2007; Bailleul et al., 2010; Klughammer et al., 2013; Johnson and Ruban, 2014). The thylakoid membrane potential during photosynthesis is defined as the total rapid (less than 1 s) change in the ECS signal (ECSt) upon rapidly switching off AL from steady state, which reflects the light-dark difference in proton motive force, and includes two components: transmembrane differences in the concentration of protons (ΔpH) and in the electric field (ΔΨ; Sacksteder and Kramer, 2000; Cruz et al., 2001, 2005; Baker et al., 2007). In this study, the values of ECSt were normalized by dividing the magnitude of ECS decay in dark-interval relaxation kinetics (DIRK) analysis by the magnitude of ECS induced by a 10-μs single-turnover flash (Klughammer et al., 2013). The initial decay rate of the ECS signal following light-to-dark transitions can be used to estimate relative light-driven proton flux through the chloroplast ATP synthase (H^+ efflux rate [v_H^+]), which is known to have a linear relationship with the photosynthetic linear electron transport rate only if there is no contribution to proton flux from cyclic electron flow around PSI (Avenson et al., 2005). Furthermore, the first-order decay time of the ECS decay in the light-to-dark transitions is required for the estimation of proton conductance in ATP synthase (g_H^+; Kanazawa and Kramer, 2002). We note that the ECS parameters are dependent on the properties of the leaves, not only the

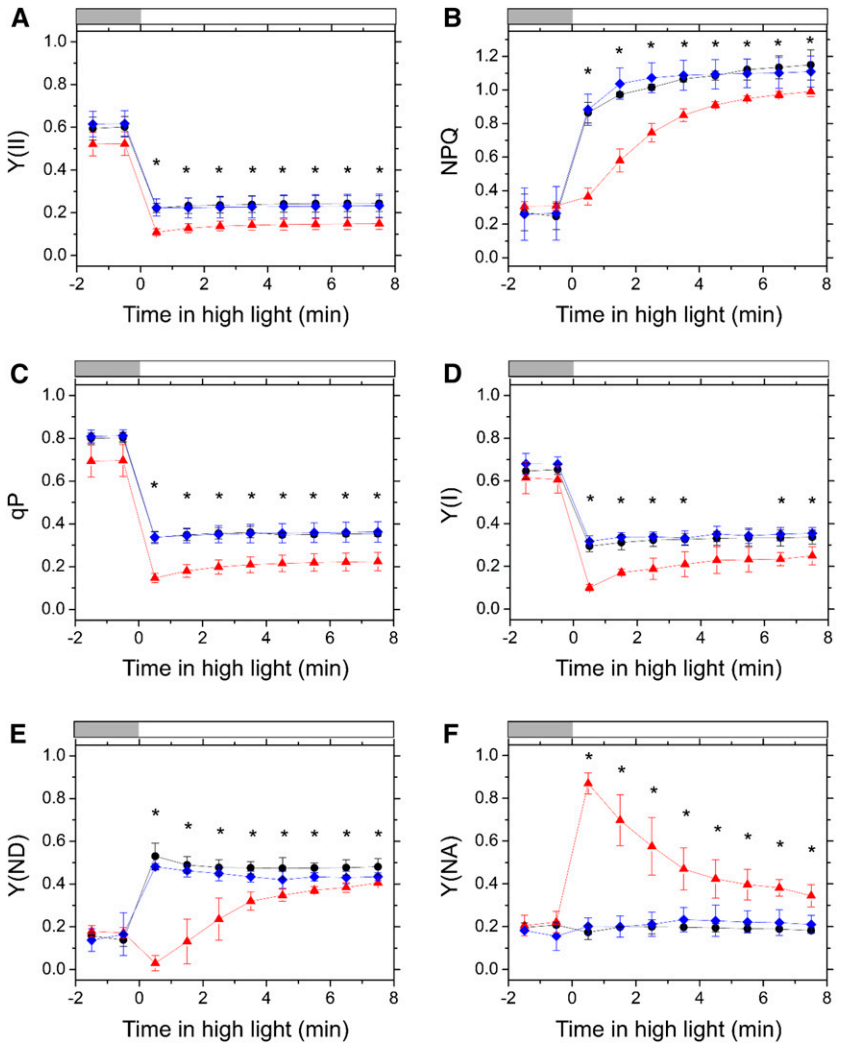

Figure 5. Time course of Y(II) (A), NPQ (B), qP (C), Y(I) (D), Y(ND) (E), and Y(NA) (F) in the transition from moderate light (200 μmol photons m^{-2} s^{-1}; light gray bars) to high light (840 μmol photons m^{-2} s^{-1}; white bars) in Tak-1 (black circles), Δ*MpFlv1* (red triangles), and c*MpFlv1* (blue diamonds). Measurements were taken in ambient air. Data are represented as means ± SD of three independent measurements. Differences between Tak-1 and Δ*MpFlv1* were analyzed using Student's *t* test. Asterisks indicate statistically significant differences between Tak-1 and Δ*MpFlv1* at $P < 0.05$.

density of chloroplasts but also the content of light-harvesting complexes that house the shifted pigments.

A lack of FLV had some impact on the ECS parameters during the transition to high light in *M. polymorpha*. The representative original kinetics of the ECS signal following light-to-dark transitions in Tak-1 and Δ*MpFlv1* are shown in Supplemental Figure S4 and were utilized to estimate the ECS parameters of the following results. In response to high light, ECSt in Tak-1 and c*MpFlv1* first increased rapidly and thereafter decreased gradually (Fig. 6A; Supplemental Fig. S5A). Compared with Tak-1 and c*MpFlv1*, ECSt in Δ*MpFlv1* decreased just after the start of illumination with high light, which was accompanied by an increase in $g_{H'}^{+}$ and thereafter increased gradually (Fig. 6A; Supplemental Fig. S5, A and B). We divided ECSt into ΔpH and ΔΨ following the method described by Klughammer et al. (2013), indicating that, in *M. polymorpha*, FLV-mediated AEF stimulates photosynthetic linear electron flow to support the establishment of ΔpH (Fig. 6). It is still unclear why g_{H}^{+} increased in Δ*MpFlv1* just after the thalli were exposed to high light (Supplemental Fig. S5B). In contrast, V_{H}^{+} increased slightly in response to high light in all three of the plants (Supplemental Fig. S5C).

We evaluated the dependence of the relative electron transport rate at PSII (rETR), calculated as the product of Y(II) and photon flux density, and ECS parameters on photon flux density during steady-state photosynthesis in Tak-1, Δ*MpFlv1*, and c*MpFlv1* (Supplemental Figs. S6 and S7), which shows the increase in rETR uncoupled with ECSt in the range of photon flux density approximately over 200 μmol photons m^{-2} s^{-1}. Unfortunately, we could not determine the reasons for the gap between ECSt and rETR in *M. polymorpha*. In intact chloroplasts and plant leaves, cyclic electron flow within PSII drives to oxidize the PQ pool, which is sensitive to ΔpH (Miyake and Yokota, 2001; Miyake et al., 2002; Miyake and Okamura, 2003; Laisk et al., 2006). In *M. polymorpha*, FLV-mediated AEF might function in the induction of cyclic electron flow within PSII through the formation of ΔpH, resulting in the increases in Y(II) and qP (Fig. 4C; Supplemental Figs. S6, A and B, and S7, A–D). The other possibility is that changes in the ratio between components of the

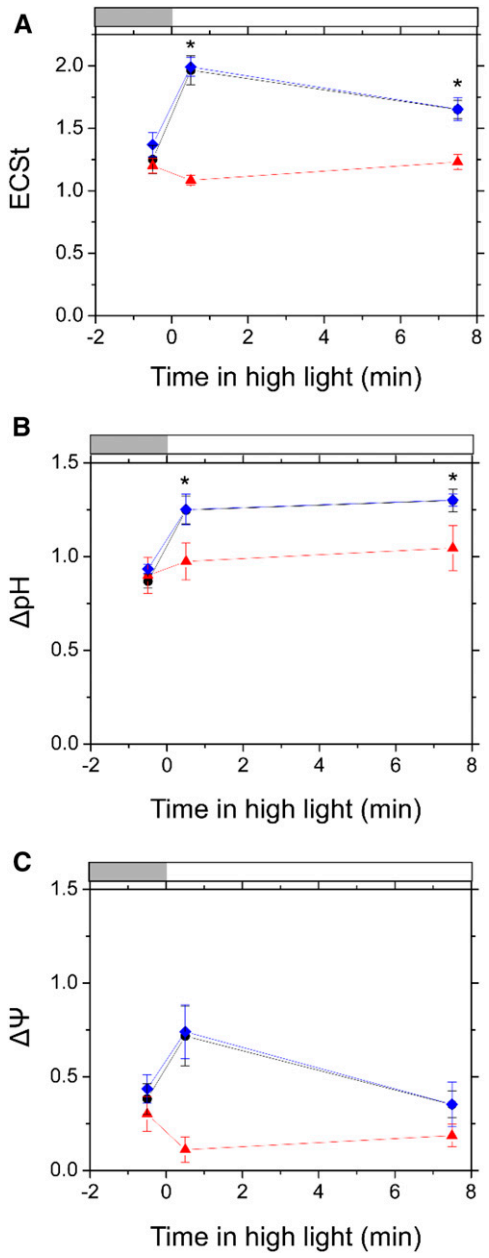

Figure 6. Time course of ECSt (A), ΔpH (B), and ΔΨ (C) during the transition from moderate light (200 μmol photons m^{-2} s^{-1}; light gray bars) to high light (830 μmol photons m^{-2} s^{-1}; white bars) in Tak-1 (black circles), Δ*MpFlv1* (red triangles), and c*MpFlv1* (blue diamonds). Measurements were taken in ambient air. Data are represented as means ± SD of three independent measurements. Differences between Tak-1 and Δ*MpFlv1* were analyzed using Student's *t* test. Asterisks indicate statistically significant differences between Tak-1 and Δ*MpFlv1* at $P < 0.05$.

photosynthetic machinery, including state transition, might be related to these results.

We also evaluated the relationship of NPQ with rETR during steady-state photosynthesis in Tak-1, Δ*MpFlv1*, and c*MpFlv1*. In plant leaves, NPQ is observed mainly in the form of energy-dependent quenching (qE), which is proportional to ΔpH but not to ΔΨ, and involves a fast (seconds to a few minutes time scale) PSII antenna reorganization (Avenson et al., 2004; Takizawa et al., 2007; Derks et al., 2015). Nevertheless, NPQ did not show the linear relationship with rETR in all three strains of *M. polymorpha* (Supplemental Fig. S8) in the range of rETR that was proportional to ΔpH (Supplemental Fig. S7D). We measured the time scale of the relaxation of NPQ after turning off AL in Tak-1 (Supplemental Fig. S9), which suggests that ΔpH-insensitive NPQ, including state transition- and photoinhibition-dependent quenching (qT and qI, respectively) (Derks et al., 2015), might occur, particularly under high light, in *M. polymorpha*.

Response of PSII Operating Efficiency to a Submerged Condition in *M. polymorpha*

We measured the responses of Y(II) to a submerged condition in Tak-1, Δ*MpFlv1*, and c*MpFlv1* using an imaging-PAM. *M. polymorpha* thalli on agar were illuminated with blue AL. After photosynthesis reached steady state, we added distilled water to completely submerge the thalli in water. During the transition to a submerged condition, decreases in Y(II) were observed in all three strains, although the change was most prominent in Δ*MpFlv1* (Fig. 7). The diffusion efficiency of CO_2 is approximately 10^4 times lower in aqueous environments compared with in the atmosphere. Submergence limits CO_2 supply to Rubisco in chloroplasts. This suppressed photosynthesis would stimulate the FLV-mediated AEF.

CONCLUSION

We clarified the physiological functions of FLV in the liverwort *M. polymorpha*, which has two genes homologous to *flv1* and *flv3* found in the cyanobacterium S. 6803. In S. 6803, most of the linear electron flow can be passed to FLV1/3 in photosynthesis induction (Helman et al., 2003; Hayashi et al., 2014; Supplemental Fig. S2), and the FLV-mediated AEF partially proceeds at steady-state photosynthesis (Helman et al., 2005). Similar to FLV in S. 6803, the gene product of *MpFlv1* drives AEF in *M. polymorpha*. In the induction phase of photosynthesis, the electron flux mediated by FLV is estimated to contribute to approximately one-quarter of the linear electron flow, at least at the photon flux density we used in this study (Fig. 2), which is smaller than that observed in S. 6803. Nevertheless, FLV-mediated AEF contributes to the oxidation of the PQ pool (Figs. 3C and 5C) and P700 (Figs. 3E and 5E). An absence of *MpFlv1* promotes the photoinhibition of PSI and PSII in *M. polymorpha* (Fig. 1). These results indicate that the physiological roles of FLV have been conserved at the current evolutional stage of basal land plants.

Liverworts probably require FLVs and their functions due to the environmental conditions of their habitats, which is implied by the results in Figure 7. Land plants are exposed to CO_2 limitations when submerged, because the diffusion rate of CO_2 in the water is much lower than in

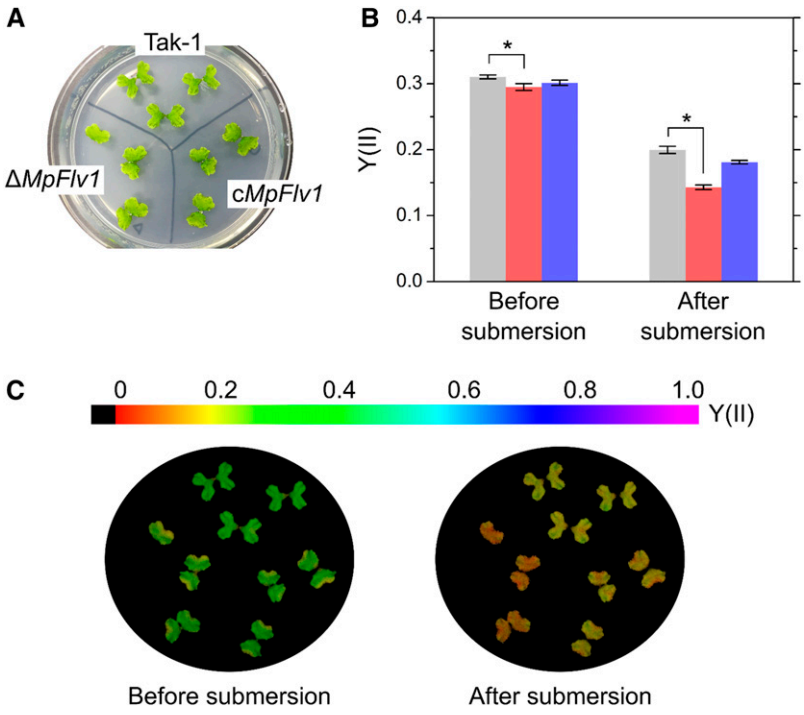

Figure 7. Responses of Y(II) to submersion in Tak-1, Δ*MpFlv1*, and c*MpFlv1*. A, Representative images of thalli on an agar medium. B, Y(II) in Tak-1 (light gray bars), Δ*MpFlv1* (pale red bars), and c*MpFlv1* (pale blue bars) before and 20 s after submersion at steady-state photosynthesis. Data are represented as means ± SD of three independent measurements. Differences between Tak-1 and Δ*MpFlv1* were analyzed using Student's *t* test. Asterisks indicate statistically significant differences between Tak-1 and Δ*MpFlv1* at $P < 0.05$. C, Representative fluorescence images of Y(II) before and 20 s after submersion at steady-state photosynthesis. Photon flux density of blue AL was adjusted to 240 μmol photons m^{-2} s^{-1}.

the atmosphere. Generally, in C_3 plants exposed to low-CO_2 conditions, photorespiration functions as an alternative electron sink to replace photosynthesis (Kozaki and Takeba, 1996; Takahashi et al., 2007), which contributes to the dissipation of excess photon energy and suppresses photooxidative damage. However, in aqueous conditions, the efficiency of ribulose 1,5-bisphosphate oxygenation catalyzed by Rubisco is low, because the affinity of ribulose 1,5-bisphosphate oxygenation reactions for oxygen, K_m for oxygen, ranges from 250 to 450 μM oxygen (Jordan and Ogren, 1981). The concentration of oxygen in the water equilibrated with the atmosphere is about 250 μM at 25°C. These facts imply that the photorespiration rate is limited by the supply of oxygen from the atmosphere, and Rubisco cannot turn over at the maximum rate under these conditions. On the other hand, K_m for oxygen in FLV reactions is below a few micromolar oxygen (Vicente et al., 2002; Shimakawa et al., 2015), and FLV catalyzes the reduction of oxygen to water at its maximum rate in the water. In fact, in some species of cyanobacteria (S. 6803, *Synechococcus elongatus* PCC 7942, and *Synechococcus* sp. PCC 7002), under suppressed photosynthesis conditions equilibrated with air, AEF is driven by FLVs, not by photorespiration (Hayashi et al., 2014; Shimakawa et al., 2015, 2016b; Shaku et al., 2016). Furthermore, some eukaryotic algae, including the green alga *Chlamydomonas reinhardtii* and the diatom *Phaeodactylum tricornutum*, do not utilize photorespiration as the main alternative electron sink under suppressed photosynthesis conditions (Shimakawa et al., 2016a, 2017). These facts suggest that oxygenic phototrophs that reside in or are exposed to aqueous environments use FLV in AEF to oxidize P700 in PSI. Recently, the moss *Physcomitrella patens* was reported to show FLV-mediated AEF, similar to *M. polymorpha* (Gerotto et al., 2016). The physiological functions of FLV may be conserved in whole bryophytes.

Here, we propose a model of the mechanisms involved in oxidizing P700 for the suppression of photooxidative damage in PSI derived from ROS in the liverwort *M. polymorpha* (Fig. 8), which appears to be broadly applicable to various oxygenic phototrophs, with the exception of the extent of FLV activity. In angiosperms, which generally do not possess FLV, this mechanism might be replaced with other molecular mechanisms, including the photorespiratory C_2 cycle, plastidial terminal oxidase, the Mehler-ascorbate peroxidase pathway, cyclic electron flow (including chloroplast NADPH dehydrogenase and ferredoxin-quinone reductase), and

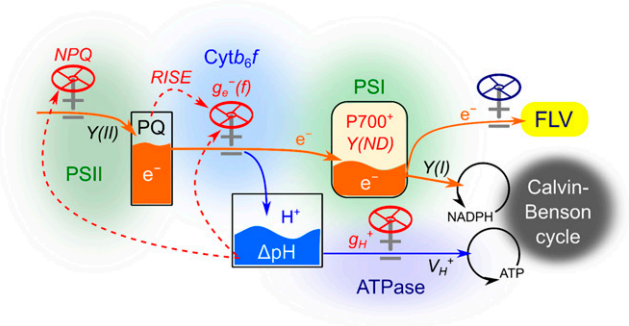

Figure 8. Model of the system for P700 oxidation to alleviate photooxidative damage to PSI in *M. polymorpha*. Photosynthetic linear electron flow is indicated by orange arrows. Blue arrows indicate proton flux. Red dashed arrows represent signal pathways regulating flux valves. pmf, Proton motive force. Details are described in the text.

malate dehydrogenase. Additionally, electron transport in the cytochrome b_6/f complex also is suppressed by sensing the redox state of the PQ pool in the reduction-induced suppression of electron flow (RISE) system, which has been characterized in the cyanobacterium *Synechococcus elongatus* PCC 7942 (Shaku et al., 2016) but not yet in photosynthetic eukaryotes. In the RISE system, accumulation of the reduced form of PQ inhibits the Q cycle in cytochrome b_6/f. That is, RISE can oxidize P700, where no limitation of the acceptor side of PSI is required as a prerequisite. The physiological functions of RISE in *M. polymorpha* await investigation in future studies. We note that there should be strategic diversity in oxygenic phototrophs commensurate with their survival on the earth.

MATERIALS AND METHODS

Culture and Growth Conditions of *Marchantia polymorpha*

A male accession of *M. polymorpha*, Tak-1, was asexually maintained according to previously described methods (Ishizaki et al., 2008). Plants were incubated on one-half-strength Gamborg's B5 agar medium (Gamborg et al., 1968) under a light/dark cycle (14 h of light, 22°C, 100 μmol photons m^{-2} s^{-1}, white fluorescent lamp/10 h of dark, 20°C). For biochemical and physiological measurements of plants, 2-week-old gemmalings were transferred from B5 agar medium onto moist vermiculite.

Targeted Gene Knockout of *MpFlv1*

To generate the *MpFlv1*-targeting vector, pJHY-TMp1 was used (Ishizaki et al., 2013). The 5′ and 3′ homology arms (4.6 and 4.5 kb, respectively) were amplified from genomic DNA extracted from Tak-1 thalli through PCR using KOD Fx Neo (Toyobo), with the primer sets T_{up} and T_{dn} used for the 5′ and 3′ homology arms, respectively (Supplemental Table S1). The PCR products of these homology arms were cloned into the *Pac*I and *Asc*I sites of pJHY-TMp1 using the In-Fusion HD Cloning Kit (Takara).

Introduction of the targeting construct into *M. polymorpha* was performed using *Rhizobium radiobactor* C58C1 GV2260, as described previously (Ishizaki et al., 2008, 2013). F1 spores generated by crossing Tak-1 and Takaragaike-2 were used for transformation. Isogenic lines (designated as G_1 lines) were obtained by isolating gemmae, which develop from single cells, and were screened for gene-targeted lines to use as Δ*MpFlv1* by genotyping using a previously described method (Ishizaki et al., 2013; Supplemental Fig. S1).

Complementation Lines of Δ*MpFlv1*

To generate complementation lines of Δ*MpFlv1*, a binary vector, pMpGWB306, harboring a mutated acetolactate synthase gene that confers chlorosulfuron resistance was used (Ishizaki et al., 2015). The coding region of *MpFlv1* was amplified from cDNA from Tak-1 through PCR using KOD plus Neo (Toyobo) with the primer set C (Supplemental Table S1) and was then cloned into pENTR/D-TOPO (Thermo Fisher Scientific). The resultant *MpFlv1* cassette was cloned into pMpGWB306 using LR Clonase II (Thermo Fisher Scientific) according to the manufacturer's protocol. The inserted *MpFlv1* was driven by the cauliflower mosaic virus 35S promoter (Ishizaki et al., 2015). Complementation lines were generated by transforming the resulting binary plasmids into regenerating thalli of Δ*MpFlv1*, as described previously (Kubota et al., 2013). Several transformants were obtained through selection with chlorosulfuron and used as c*MpFlv1* lines.

Measurement of *MpFlv1* Transcripts

Reverse transcription-PCR was performed using KOD Fx Neo (Toyobo) with cDNA from Tak-1, Δ*MpFlv1*, and c*MpFlv1*. We used the *Actin* gene (*Mapoly0016s0137*) as a reference gene. The primer sets used (RT_{FLV} and RT_{ACT}) are listed in Supplemental Table S1.

Measurements of Chl and Nitrogen

The contents of Chl *a* and *b* in the *M. polymorpha* thalli were spectrophotometrically measured using a U-2800A spectrophotometer (Hitachi). For the measurement, extracts of thalli were obtained through incubation in 100% (v/v) *N*,*N*-dimethylformamide overnight. Both the Chl *a* and *b* contents in each extract were determined using the methods of Porra et al. (1989).

To measure nitrogen, *M. polymorpha* thalli were dried overnight at 60°C and then digested via Kjeldahl digestion with sulfuric acid. Total nitrogen contents were determined with Nessler's reagent after adding sodium potassium tartrate (Shimakawa et al., 2014).

Measurements of Oxygen Exchange and Chl Fluorescence

Oxygen exchange was monitored simultaneously with Chl fluorescence. Thalli (2−5 cm^2) were set in the oxygen electrode chamber (LD2/3; Hansatech), and Chl fluorescence was monitored using a Junior-PAM Chl fluorometer (Walz) through a light-guided plastic-fiber set into the oxygen electrode chamber (Sejima et al., 2016). The temperature of the chamber was set to 25°C. Red AL was illuminated from the top of the oxygen electrode chamber, and the photon flux densities were adjusted to the values indicated in the corresponding figure legends. Since the oxygen electrode chamber was a closed system, CO_2-saturated conditions were simulated by placing a fabric mat wetted with 1 M $NaHCO_3$ solution below the intact thalli to supply CO_2 at a concentration of approximately 1% (v/v). The photosynthetic parameters in PSII were calculated using Chl fluorescence parameters as described below (see "Measurements of Chl Fluorescence and P700").

For the measurements of oxygen exchange and Chl fluorescence in the liquid phase, we used an oxygen electrode chamber (DW2/2; Hansatech), a PAM-101 Chl fluorometer (Walz), and cyanobacterial cells grown under high-CO_2 conditions according to the methods of Shimakawa et al. (2016a). The reaction mixture (2 mL) contained 50 mM HEPES (pH 7.5), 10 mM $NaHCO_3$, and the cyanobacterial cells (10 μg Chl mL^{-1}). Cells were illuminated with red AL ($620 < \lambda < 695$ nm, 240 μmol photons m^{-2} s^{-1}) at 25°C. During the measurements, the reaction mixture was stirred with a magnetic microstirrer. Pulse-modulated excitation was achieved using a light-emitting diode lamp with a peak emission of 650 nm. Modulated fluorescence was measured at $\lambda > 710$ nm (Schott RG9 long-pass filter). The photosynthetic parameters in PSII were calculated using Chl fluorescence parameters, as described below (see "Measurements of Chl Fluorescence and P700").

Measurements of Chl Fluorescence and P700

Both Chl fluorescence and $P700^+$ were measured simultaneously using a Dual-PAM-100 fluorometer (Walz). In this measurement, we used a 3010 DUAL gas-exchange leaf chamber (Walz). Ambient air was saturated with water vapor at 18°C ± 0.1°C, and the leaf temperature was maintained at 25°C. The photosynthetic parameters in PSII were calculated using Chl fluorescence parameters as follows (Baker, 2008): $F_v/F_m = (F_m - F_o)/F_m$, $Y(II) = (F_m' - F')/F_m'$, $NPQ = (F_m - F_m')/F_m'$, and $qP = (F_m' - F')/(F_m' - F_o)$, where F_o, minimum fluorescence from a dark-adapted leaf; F_m, maximum fluorescence from a dark-adapted leaf; F_m', maximum fluorescence from a light-adapted leaf; and F', fluorescence emission from a light-adapted leaf. Pulse amplitude-modulated measuring light (0.1 μmol photons m^{-2} s^{-1}) was applied to determine F_o. Short-saturation pulses (10,000 μmol photons m^{-2} s^{-1}, 300 ms) were applied to determine F_m and F_m'.

The photosynthetic parameters in PSI were calculated from the redox state of P700 as follows (Klughammer and Schreiber, 1994; Schreiber and Klughammer, 2008): $Y(I) = (P_m' - P)/P_m$, $Y(NA) = (P_m - P_m')/P_m$, and $Y(ND) = P/P_m$, where P_m, total amount of photooxidizable P700; P_m', maximum amount of photooxidized P700 by a saturation pulse; and P, amount of photooxidized P700 at steady state. Red AL was used to measure the photosynthetic parameters at photon flux densities, as indicated in the corresponding figure legends.

For measurements in the absence of oxygen, pure N_2 gas was prepared and saturated with water vapor at 18°C ± 0.1°C.

During analysis with an Imaging-PAM (M-Series; Walz), pulse-modulated excitation, actinic illumination, and saturation pulses were achieved with a blue light-emitting diode lamp with a peak emission of 450 nm. Images of the fluorescence parameters were displayed with the help of a false-color code ranging from black (0) through red, yellow, green, blue, and pink (1; Singh et al., 2013).

Measurement of ECS

ECS was measured using a Dual-PAM-100 fluorometer equipped with a P515-analysis module (Klughammer et al., 2013). In this measurement, we used a

3010 DUAL gas-exchange leaf chamber (Walz). Ambient air was saturated with water vapor at 18°C ± 0.1°C, and the leaf temperature was maintained at 25°C. ECSt, g_H^+ in ATP synthase, and V_H^+ were measured through DIRK analysis, as described by Sacksteder and Kramer (2000) and Baker et al. (2007). For the DIRK analysis, we set the transient dark (600 ms) during illumination with AL. We measured the extent of the change in ECS as ECSt and the half-life of ECS decay for the calculation of $g_H^+(s^{-1})$. During the transient dark, V_H^+ was estimated from the initial decay of ECS. The values of ECSt were normalized by dividing the magnitude of ECS decay in DIRK analysis by the magnitude of ECS induced by a 10-μs single-turnover flash (Klughammer et al., 2013). In separate experiments, ECSt was divided into ΔpH and ΔΨ following the methods of Klughammer et al. (2013).

Statistical Analysis

We used Student's *t* test to detect differences. All statistical analyses were performed using Microsoft Excel 2010 (Microsoft) and JMP8 (SAS Institute).

Accession Numbers

The sequence data used in this study are originated from a preliminary genome database.

Supplemental Data

The following supplemental materials are available.

Supplemental Figure S1. Strategy for targeted disruption of the *MpFlv1* locus and analysis of homologous recombination events.

Supplemental Figure S2. Time course of gross photosynthetic oxygen evolution rates and Y(II) in the induction phase of photosynthesis in S. 6803 wild type and Δ*flv1/3*.

Supplemental Figure S3. Dependence of gross photosynthetic oxygen evolution rates and Y(II) on photon flux density at steady-state photosynthesis in Tak-1, Δ*MpFlv1*, and c*MpFlv1*.

Supplemental Figure S4. Representative original traces of dark-interval relaxation kinetics of ECS in Tak-1 and Δ*MpFlv1*.

Supplemental Figure S5. Time course of ECSt, g_H^+, and V_H^+ in the transition from moderate to high light in Tak-1, Δ*MpFlv1*, and c*MpFlv1*.

Supplemental Figure S6. Dependence of rETR, ECSt, g_H^+, and V_H^+ on photon flux density at steady-state photosynthesis in Tak-1, Δ*MpFlv1*, and c*MpFlv1*.

Supplemental Figure S7. Dependence of ECSt, ΔpH, and ΔΨ on photon flux density and the relationship of ECSt, ΔpH, and ΔΨ to the rETR at steady-state photosynthesis in Tak-1, Δ*MpFlv1*, and c*MpFlv1*.

Supplemental Figure S8. Relationship of NPQ to the rETR at steady-state photosynthesis in Tak-1, Δ*MpFlv1*, and c*MpFlv1*.

Supplemental Figure S9. Relaxation of NPQ after transition to the dark.

Supplemental Table S1. Primers used in this study.

Received July 5, 2016; accepted January 31, 2017; published February 2, 2017.

LITERATURE CITED

Allahverdiyeva Y, Mustila H, Ermakova M, Bersanini L, Richaud P, Ajlani G, Battchikova N, Cournac L, Aro EM (2013) Flavodiiron proteins Flv1 and Flv3 enable cyanobacterial growth and photosynthesis under fluctuating light. Proc Natl Acad Sci USA **110:** 4111–4116

Asada K (1999) The water-water cycle in chloroplasts: scavenging of active oxygens and dissipation of excess photons. Annu Rev Plant Physiol Plant Mol Biol **50:** 601–639

Avenson TJ, Cruz JA, Kanazawa A, Kramer DM (2005) Regulating the proton budget of higher plant photosynthesis. Proc Natl Acad Sci USA **102:** 9709–9713

Avenson TJ, Cruz JA, Kramer DM (2004) Modulation of energy-dependent quenching of excitons in antennae of higher plants. Proc Natl Acad Sci USA **101:** 5530–5535

Badger MR, Spalding MH (2000) CO_2 acquisition, concentration and fixation in cyanobacteria and algae. *In* RC Leegood, TD Sharkey, S von Caemmerer, eds, Photosynthesis: Physiology and Metabolism. Springer, Dordrecht, The Netherlands, pp 369–397

Bailleul B, Cardol P, Breyton C, Finazzi G (2010) Electrochromism: a useful probe to study algal photosynthesis. Photosynth Res **106:** 179–189

Baker NR (2008) Chlorophyll fluorescence: a probe of photosynthesis in vivo. Annu Rev Plant Biol **59:** 89–113

Baker NR, Harbinson J, Kramer DM (2007) Determining the limitations and regulation of photosynthetic energy transduction in leaves. Plant Cell Environ **30:** 1107–1125

Boardman NK (1977) Comparative photosynthesis of sun and shade plants. Annu Rev Plant Physiol **28:** 355–377

Bowman JL, Floyd SK, Sakakibara K (2007) Green genes: comparative genomics of the green branch of life. Cell **129:** 229–234

Cazzaniga S, Li Z, Niyogi KK, Bassi R, Dall'Osto L (2012) The Arabidopsis *szl1* mutant reveals a critical role of β-carotene in photosystem I photoprotection. Plant Physiol **159:** 1745–1758

Cruz JA, Kanazawa A, Treff N, Kramer DM (2005) Storage of light-driven transthylakoid proton motive force as an electric field ($\Delta\psi$) under steady-state conditions in intact cells of Chlamydomonas reinhardtii. Photosynth Res **85:** 221–233

Cruz JA, Sacksteder CA, Kanazawa A, Kramer DM (2001) Contribution of electric field ($\Delta\ \psi$) to steady-state transthylakoid proton motive force (*pmf*) in vitro and in vivo: control of *pmf* parsing into $\Delta\ \psi$ and Δ pH by ionic strength. Biochemistry **40:** 1226–1237

Derks A, Schaven K, Bruce D (2015) Diverse mechanisms for photoprotection in photosynthesis: dynamic regulation of photosystem II excitation in response to rapid environmental change. Biochim Biophys Acta **1847:** 468–485

Fischer BB, Hideg É, Krieger-Liszkay A (2013) Production, detection, and signaling of singlet oxygen in photosynthetic organisms. Antioxid Redox Signal **18:** 2145–2162

Gamborg OL, Miller RA, Ojima K (1968) Nutrient requirements of suspension cultures of soybean root cells. Exp Cell Res **50:** 151–158

Gerotto C, Alboresi A, Meneghesso A, Jokel M, Suorsa M, Aro EM, Morosinotto T (2016) Flavodiiron proteins act as safety valve for electrons in *Physcomitrella patens*. Proc Natl Acad Sci USA **113:** 12322–12327

Hayashi R, Shimakawa G, Shaku K, Shimizu S, Akimoto S, Yamamoto H, Amako K, Sugimoto T, Tamoi M, Makino A, et al (2014) O_2-dependent large electron flow functioned as an electron sink, replacing the steady-state electron flux in photosynthesis in the cyanobacterium *Synechocystis* sp. PCC 6803, but not in the cyanobacterium *Synechococcus* sp. PCC 7942. Biosci Biotechnol Biochem **78:** 384–393

Helman Y, Barkan E, Eisenstadt D, Luz B, Kaplan A (2005) Fractionation of the three stable oxygen isotopes by oxygen-producing and oxygen-consuming reactions in photosynthetic organisms. Plant Physiol **138:** 2292–2298

Helman Y, Tchernov D, Reinhold L, Shibata M, Ogawa T, Schwarz R, Ohad I, Kaplan A (2003) Genes encoding A-type flavoproteins are essential for photoreduction of O_2 in cyanobacteria. Curr Biol **13:** 230–235

Ishizaki K, Chiyoda S, Yamato KT, Kohchi T (2008) *Agrobacterium*-mediated transformation of the haploid liverwort *Marchantia polymorpha* L., an emerging model for plant biology. Plant Cell Physiol **49:** 1084–1091

Ishizaki K, Johzuka-Hisatomi Y, Ishida S, Iida S, Kohchi T (2013) Homologous recombination-mediated gene targeting in the liverwort *Marchantia polymorpha* L. Sci Rep **3:** 1532

Ishizaki K, Nishihama R, Ueda M, Inoue K, Ishida S, Nishimura Y, Shikanai T, Kohchi T (2015) Development of Gateway binary vector series with four different selection markers for the liverwort *Marchantia polymorpha*. PLoS ONE **10:** e0138876

Johnson MP, Ruban AV (2014) Rethinking the existence of a steady-state $\Delta\psi$ component of the proton motive force across plant thylakoid membranes. Photosynth Res **119:** 233–242

Jordan DB, Ogren WL (1981) Species variation in the specificity of ribulose bisphosphate carboxylase/oxygenase. Nature **291:** 513–515

Kanazawa A, Kramer DM (2002) *In vivo* modulation of nonphotochemical exciton quenching (NPQ) by regulation of the chloroplast ATP synthase. Proc Natl Acad Sci USA **99:** 12789–12794

Klughammer C, Schreiber U (1994) An improved method, using saturating light pulses, for the determination of photosystem I quantum yield via $P700^+$-absorbance changes at 830 nm. Planta **192:** 261–268

Klughammer C, Siebke K, Schreiber U (2013) Continuous ECS-indicated recording of the proton-motive charge flux in leaves. Photosynth Res **117:** 471–487

Kozaki A, Takeba G (1996) Photorespiration protects C3 plants from photooxidation. Nature **384:** 557–560

Kramer DM, Sacksteder CA, Cruz JA (1999) How acidic is the lumen? Photosynth Res **60:** 151–163

Krause GH, Köster S, Wong SC (1985) Photoinhibition of photosynthesis under anaerobic conditions studied with leaves and chloroplasts of *Spinacia oleracea* L. Planta **165:** 430–438

Krieger-Liszkay A (2005) Singlet oxygen production in photosynthesis. J Exp Bot **56:** 337–346

Kubota A, Ishizaki K, Hosaka M, Kohchi T (2013) Efficient *Agrobacterium*-mediated transformation of the liverwort *Marchantia polymorpha* using regenerating thalli. Biosci Biotechnol Biochem **77:** 167–172

Laisk A, Eichelmann H, Oja V, Rasulov B, Rämma H (2006) Photosystem II cycle and alternative electron flow in leaves. Plant Cell Physiol **47:** 972–983

Miyake C (2008) Coupled regulation of cyclic electron flow around PSI with photosynthesis: its contribution to non-photochemical quenching evidenced with transplastomic tobacco plants over-expressing ferredoxin in chloroplasts. *In* JF Allen, E Gantt, JH Golbeck, B Osmond, eds, Photosynthesis: Energy from the Sun. 14th International Congress on Photosynthesis. Springer, Dordrecht, The Netherlands, pp 923–927

Miyake C (2010) Alternative electron flows (water-water cycle and cyclic electron flow around PSI) in photosynthesis: molecular mechanisms and physiological functions. Plant Cell Physiol **51:** 1951–1963

Miyake C, Okamura M (2003) Cyclic electron flow within PSII protects PSII from its photoinhibition in thylakoid membranes from spinach chloroplasts. Plant Cell Physiol **44:** 457–462

Miyake C, Yokota A (2001) Cyclic flow of electrons within PSII in thylakoid membranes. Plant Cell Physiol **42:** 508–515

Miyake C, Yonekura K, Kobayashi Y, Yokota A (2002) Cyclic electron flow within PSII functions in intact chloroplasts from spinach leaves. Plant Cell Physiol **43:** 951–957

Porra R, Thompson W, Kriedelman P (1989) Determination of accurate extraction and simultaneously equation for assaying chlorophyll *a* and *b* extracted with different solvents: verification of the concentration of chlorophyll standards by atomic absorption spectroscopy. Biochim Biophys Acta **975:** 384–394

Raven JA, Osborne BA, Johnston AM (1985) Uptake of CO_2 by aquatic vegetation. Plant Cell Environ **8:** 417–425

Rutherford AW, Osyczka A, Rappaport F (2012) Back-reactions, short-circuits, leaks and other energy wasteful reactions in biological electron transfer: redox tuning to survive life in O_2. FEBS Lett **586:** 603–616

Sacksteder CA, Kramer DM (2000) Dark-interval relaxation kinetics (DIRK) of absorbance changes as a quantitative probe of steady-state electron transfer. Photosynth Res **66:** 145–158

Schreiber U, Klughammer C (2008) Saturation pulse method for assessment of energy conversion in PSI. PAM Appl Notes **1:** 11–14

Sejima T, Hanawa H, Shimakawa G, Takagi D, Suzuki Y, Fukayama H, Makino A, Miyake C (2016) Post-illumination transient O_2-uptake is driven by photorespiration in tobacco leaves. Physiol Plant **156:** 227–238

Sejima T, Takagi D, Fukayama H, Makino A, Miyake C (2014) Repetitive short-pulse light mainly inactivates photosystem I in sunflower leaves. Plant Cell Physiol **55:** 1184–1193

Shaku K, Shimakawa G, Hashiguchi M, Miyake C (2016) Reduction-induced suppression of electron flow (RISE) in the photosynthetic electron transport system of *Synechococcus elongatus* PCC 7942. Plant Cell Physiol **57:** 1443–1453

Shimakawa G, Akimoto S, Ueno Y, Wada A, Shaku K, Takahashi Y, Miyake C (2016a) Diversity in photosynthetic electron transport under $[CO_2]$-limitation: the cyanobacterium *Synechococcus* sp. PCC 7002 and green alga *Chlamydomonas reinhardtii* drive an O_2-dependent alternative electron flow and non-photochemical quenching of chlorophyll fluorescence during CO_2-limited photosynthesis. Photosynth Res **130:** 293–305

Shimakawa G, Hasunuma T, Kondo A, Matsuda M, Makino A, Miyake C (2014) Respiration accumulates Calvin cycle intermediates for the rapid start of photosynthesis in *Synechocystis* sp. PCC 6803. Biosci Biotechnol Biochem **78:** 1997–2007

Shimakawa G, Matsuda Y, Nakajima K, Tamoi M, Shigeoka S, Miyake C (2017) Diverse strategies of O_2 usage for preventing photo-oxidative damage under CO_2 limitation during algal photosynthesis. Sci Rep **7:** 41022

Shimakawa G, Shaku K, Miyake C (2016b) Oxidation of P700 in photosystem I is essential for the growth of cyanobacteria. Plant Physiol **172:** 1443–1450

Shimakawa G, Shaku K, Nishi A, Hayashi R, Yamamoto H, Sakamoto K, Makino A, Miyake C (2015) FLAVODIIRON2 and FLAVODIIRON4 proteins mediate an oxygen-dependent alternative electron flow in *Synechocystis* sp. PCC 6803 under CO_2-limited conditions. Plant Physiol **167:** 472–480

Singh R, Ranjan S, Nayaka S, Pathre UV, Shirke PA (2013) Functional characteristics of a fruticose type of lichen, *Stereocaulon foliolosum* Nyl. in response to light and water stress. Acta Physiol Plant **35:** 1605–1615

Takagi D, Takumi S, Hashiguchi M, Sejima T, Miyake C (2016) Superoxide and singlet oxygen produced within the thylakoid membranes both cause photosystem I photoinhibition. Plant Physiol **171:** 1626–1634

Takahashi S, Bauwe H, Badger M (2007) Impairment of the photorespiratory pathway accelerates photoinhibition of photosystem II by suppression of repair but not acceleration of damage processes in Arabidopsis. Plant Physiol **144:** 487–494

Takizawa K, Cruz JA, Kanazawa A, Kramer DM (2007) The thylakoid proton motive force *in vivo*: quantitative, non-invasive probes, energetics, and regulatory consequences of light-induced *pmf*. Biochim Biophys Acta **1767:** 1233–1244

Vicente JB, Gomes CM, Wasserfallen A, Teixeira M (2002) Module fusion in an A-type flavoprotein from the cyanobacterium *Synechocystis* condenses a multiple-component pathway in a single polypeptide chain. Biochem Biophys Res Commun **294:** 82–87

Witt HT (1979) Energy conversion in the functional membrane of photosynthesis: analysis by light pulse and electric pulse methods. The central role of the electric field. Biochim Biophys Acta **505:** 355–427

Yamamoto H, Takahashi S, Badger MR, Shikanai T (2016) Artificial remodelling of alternative electron flow by flavodiiron proteins in Arabidopsis. Nat Plants **2:** 16012

Zhang P, Eisenhut M, Brandt AM, Carmel D, Silén HM, Vass I, Allahverdiyeva Y, Salminen TA, Aro EM (2012) Operon *flv4-flv2* provides cyanobacterial photosystem II with flexibility of electron transfer. Plant Cell **24:** 1952–1971

Zivcak M, Brestic M, Kunderlikova K, Olsovska K, Allakhverdiev SI (2015a) Effect of photosystem I inactivation on chlorophyll *a* fluorescence induction in wheat leaves: does activity of photosystem I play any role in OJIP rise? J Photochem Photobiol B **152:** 318–324

Zivcak M, Brestic M, Kunderlikova K, Sytar O, Allakhverdiev SI (2015b) Repetitive light pulse-induced photoinhibition of photosystem I severely affects CO_2 assimilation and photoprotection in wheat leaves. Photosynth Res **126:** 449–463

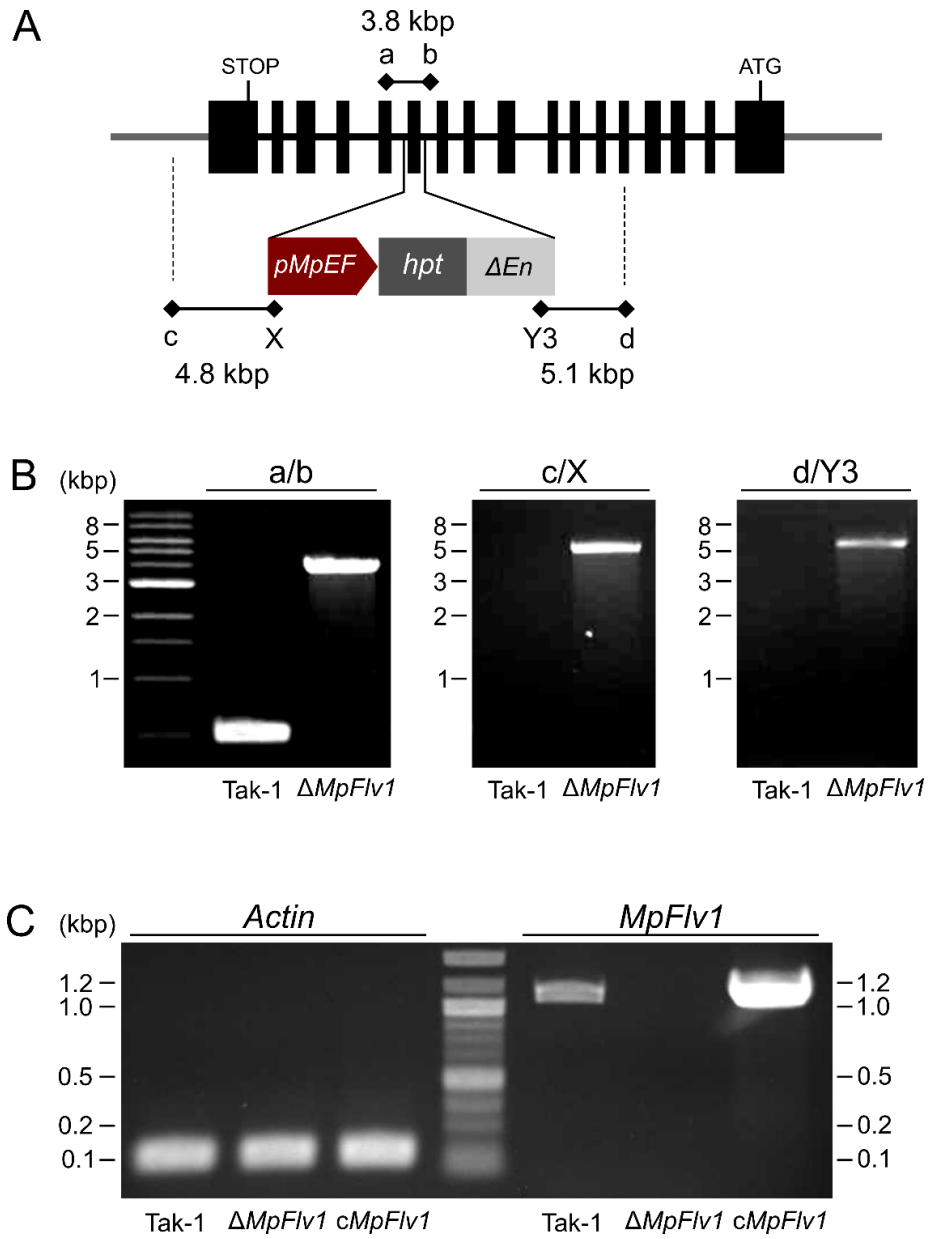

Fig. S1. Strategy for targeted disruption of the *MpFlv1* locus and analysis of homologous recombination events. (A) Schematic diagram of targeted disruption of the *MpFlv1* locus through homologous recombination. (B) Genotyping of the Δ*MpFlv1* lines. The positions of the primers used for PCR analysis are shown in Fig. S1A. (C) Reverse transcript-PCR of *MpFlv1* in Tak-1, Δ*MpFlv1*, and c*MpFlv1*.

Figure S1

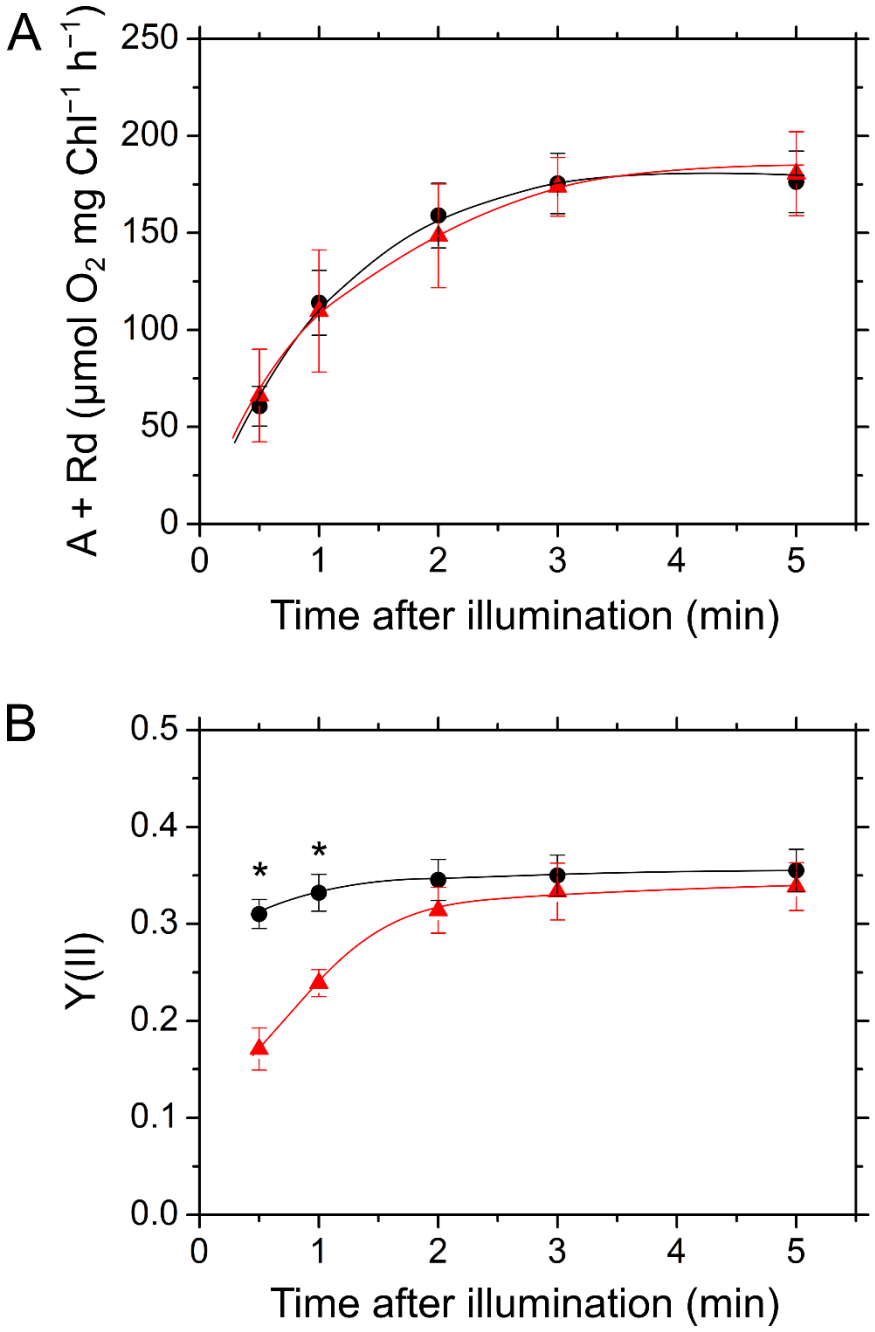

Fig. S2. Time course of gross photosynthetic O_2-evolution rates (A) and Y(II) (B) in the induction phase of photosynthesis in S. 6803 WT (black circles) and Δ*flv1/3* (red triangles). CO_2-saturated conditions were generated by adding 10 mM $NaHCO_3$ to the reaction mixture. Actinic light (240 µmol photons m^{-2} s^{-1}) was turned on at time zero. Data are represented as the mean ± SD of three independent measurements. Differences in Y(II) between S. 6803 WT and Δ*flv1/3* were analyzed using Student's *t*-test. Asterisks indicate statistically significant differences between S. 6803 and Δ*flv1/3* at $p < 0.05$.

Figure S2

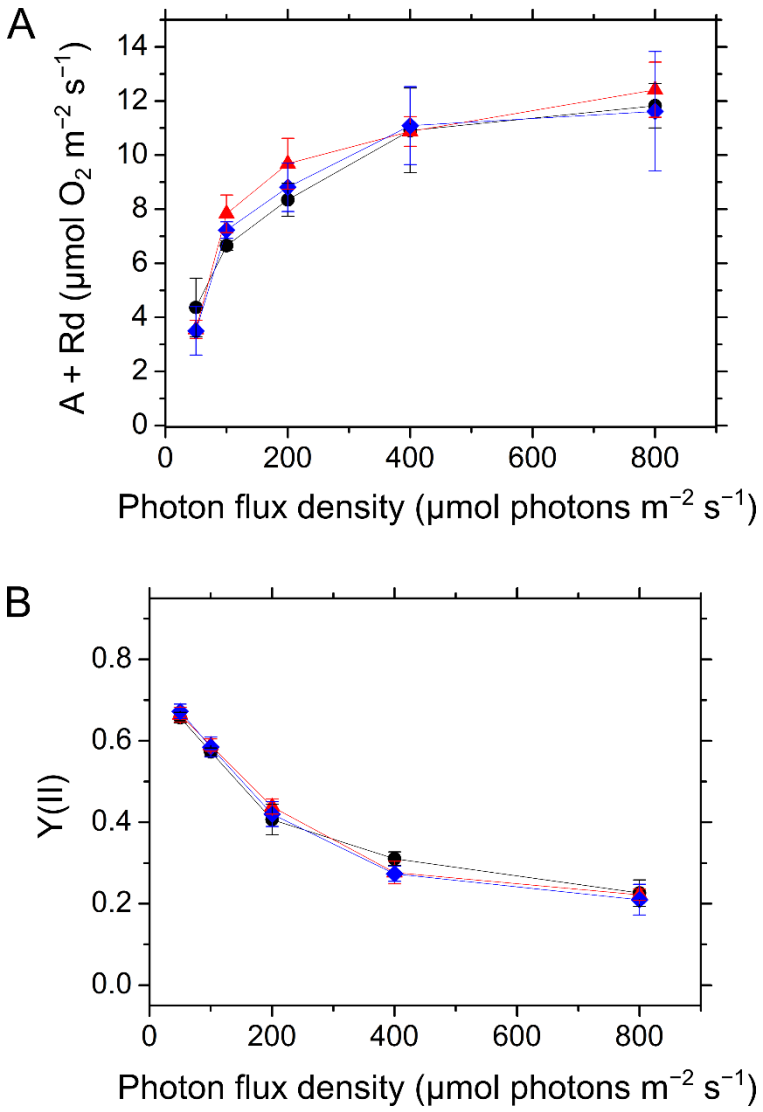

Fig. S3. Dependence of gross photosynthetic O_2-evolution rates (A) and Y(II) (B) on photon flux density at steady-state photosynthesis in Tak-1 (black circles), Δ*MpFlv1* (red triangles), and c*MpFlv1* (blue diamonds). CO_2-saturated conditions were generated by adding 1 M $NaHCO_3$ to the felt mat in the reaction chamber. Data are represented as the mean ± SD of three independent measurements.

Figure S3

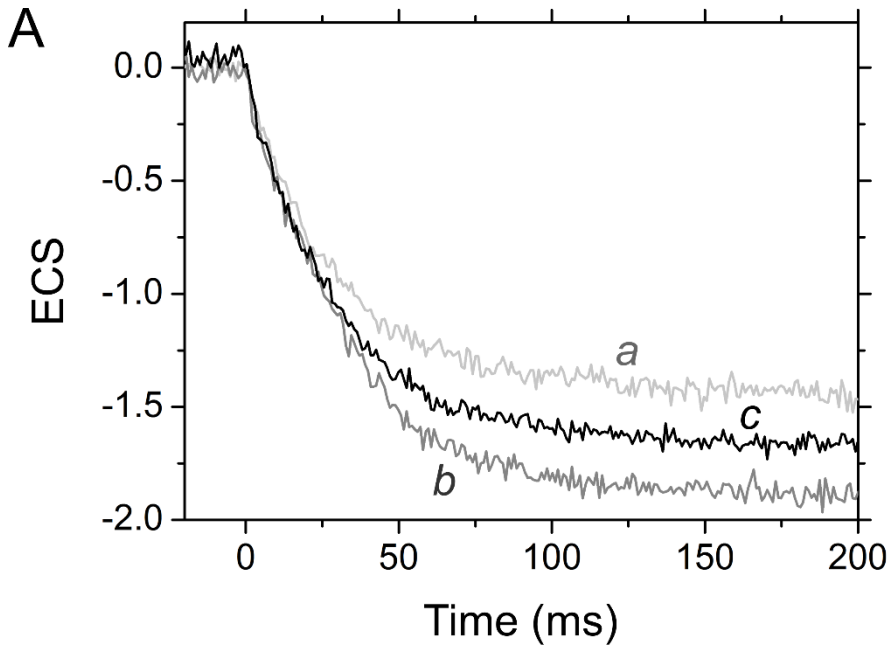

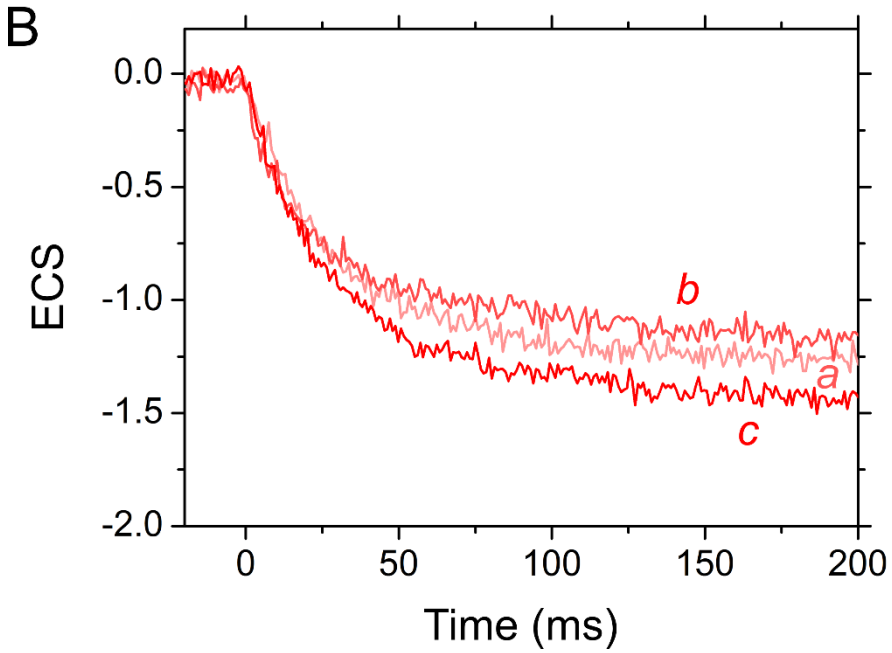

Fig. S4. The representative original traces of dark-interval relaxation kinetics of ECS in Tak-1 (A) and Δ*MpFlv1* (B) during the experiment shown in Supplemental Fig. S5. The shown traces were obtained during the transition to high light at −0.5, 0.5, and 4.5 min on the *x*-axis in Supplemental Fig. S5 (*a*, *b*, and *c* respectively). Line colors become darker over time. Actinic light was turned off at time zero.

Figure S4

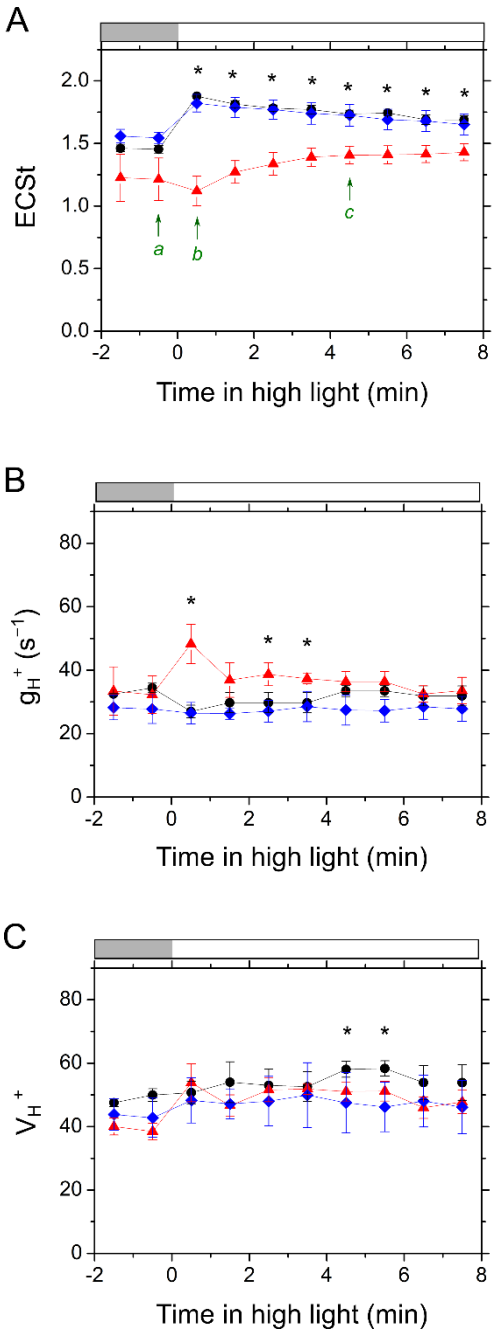

Fig. S5. Time courses of ECSt (A), g_H^+ (B), and V_H^+ (C) in the transition from moderate (180 µmol photons m^{-2} s^{-1}, light grey bars) to high (760 µmol photons m^{-2} s^{-1}, white bars) light in Tak-1 (black circles), Δ*MpFlv1* (red triangles), and c*MpFlv1* (blue diamonds). Measurements were taken under ambient air. Data are represented as the mean ± SD of three independent measurements. Differences between Tak-1 and Δ*MpFlv1* were analyzed using the Student's *t*-test. Asterisks indicate statistically significant differences between Tak-1 and Δ*MpFlv1* at $p < 0.05$. The original traces of the ECS signal at *a*, *b*, and *c* (indicated by green arrows) are shown in Supplemental Fig. S4.

Figure S5

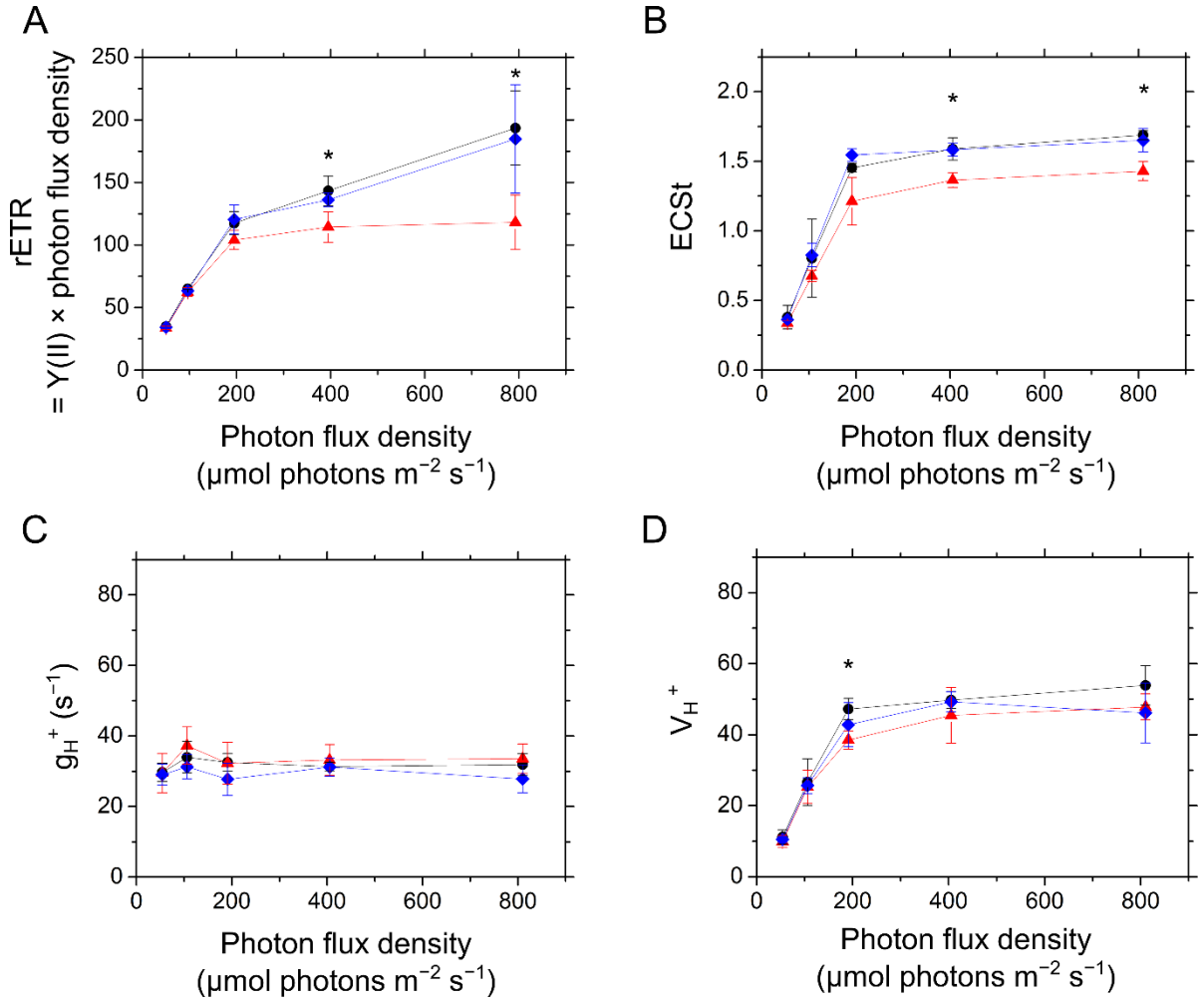

Fig. S6. Dependence of rETR (A), ECSt (B), g_H^+ (C), and V_H^+ (D) on photon flux density at steady-state photosynthesis in Tak-1 (black circles), Δ*MpFlv1* (red triangles), and c*MpFlv1* (blue diamonds). Measurements were taken in ambient air. Calculation of rETR was conducted using the data from Fig. 4A. Data are represented as the mean ± SD of three independent measurements. Differences between Tak-1 and Δ*MpFlv1* were analyzed using Student's *t*-test. Asterisks indicate statistically significant differences between Tak-1 and Δ*MpFlv1* at $p < 0.05$.

Figure S6

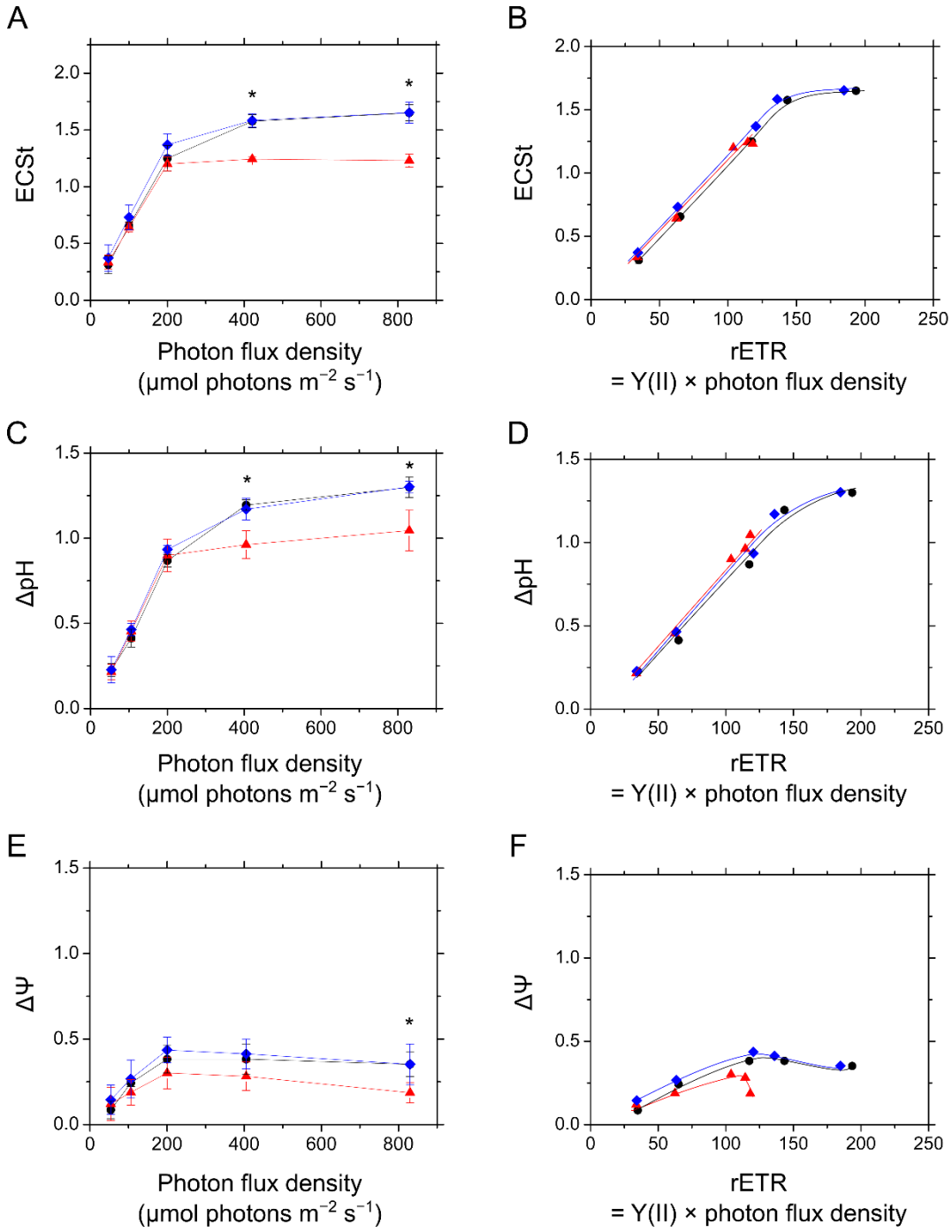

Fig. S7. Dependence of ECSt (A), ΔpH (C), and ΔΨ (E) on photon flux density and the relationship of ECSt (B), ΔpH (D), and ΔΨ (F) to rETR at steady-state photosynthesis in Tak-1 (black circles), Δ*MpFlv1* (red triangles), and c*MpFlv1* (blue diamonds). Measurements were taken in ambient air. Calculation of the rETR was conducted using the data of Fig. 4A. Respective ECS parameters were plotted on the rETR at approximately the same photon flux densities. Data are represented as the mean ± SD of three independent measurements. Differences between Tak-1 and Δ*MpFlv1* were analyzed using Student's *t*-test. Asterisks indicate statistically significant differences between Tak-1 and Δ*MpFlv1* at $p < 0.05$.

Figure S7

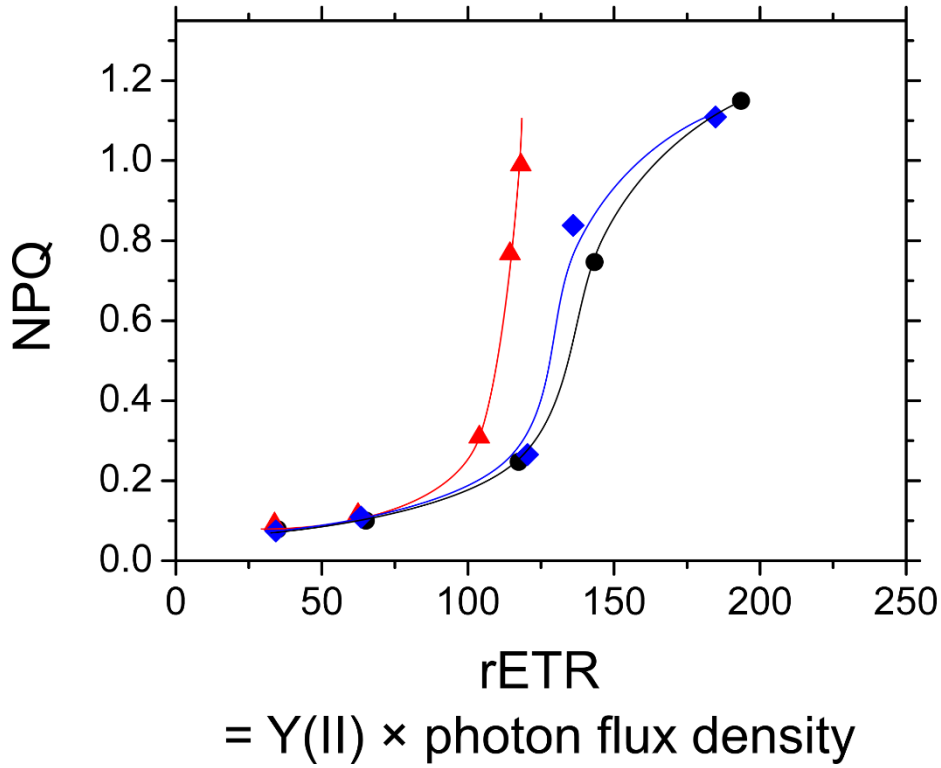

Fig. S8. Relationship of NPQ to rETR at steady-state photosynthesis in Tak-1 (black circles), Δ*MpFlv1* (red triangles), and c*MpFlv1* (blue diamonds). Measurements were taken in ambient air. Calculation of rETR was conducted using the data from Fig. 4A. NPQ from Fig. 4B was plotted on rETR at the same photon flux densities. Data are represented as the mean ± SD of three independent measurements.

Figure S8

Supplemental Table S1. Primers used in this study

Name	Sequences (5′−3′)
T_{up} F	CTAAGGTAGCGATTATCAAAAGATGCATAGTACAACAAAAGCAGA
T_{up} R	GCCCGGGCAAGCTTAGATCAAGGGTTTCGGGTTCTCG
T_{dn} F	TAAACTAGTGGCGCGGGCCTGCAGAGGCAGAAAAGAC
T_{dn} R	TTATCCCTAGGCGCGATGTGCAACAACGGGGGAAAGT
a	GGCGTAAAACCTGCCTCCTTCA
b	TGAGACGTACCACCTGCCAAGC
c	CAAAAAGTCAATGAACTGTCTGCAATCAA
d	CGGGCGATGTGCTTGATCTT
C F	CACCATGATGGCCCTTACGATGCC
C R	GTAGCGTGCTCCTGTCTTCC
RT_{FLV} F	GAATCACTCCCAAGGCGTTC
RT_{FLV} R	GAGGACGCTGTATGGACAGGC
RT_{ACT} F	GAGCGCGGTTACTCTTTCAC
RT_{ACT} R	GACCGTCAGGAAGCTCGTAG
X	GAAGGCTTCTGATTGAAGTTTCCTTTTCTG
Y3	TGGATTTGAACTTCTTTCGTATGGA

1